Natural Giesekus fluids: shear and extensional behaviour of food gum solutions in the semi-dilute regime

M.D. Torres · B. Hallmark ·L. Hilliou· D.I. Wilson

Abstract

The shear and extensional behaviour of two aqueous gum solutions, namely (i) 1-20 g/L guar gum [1]and (ii) κ/ι-hybrid carrageenan solutions (5-20 g/L), are shown to exhibit Giesekus-fluid behaviour when in the semi-dilute regime. In this regime a common set of Giesekus fluid parameters described both shear and extensional behaviour. A new analytical result describing the extension of a Giesekus fluid in the filament stretching geometry is presented. This also gave reasonable predictions of the Trouton ratio. Higher concentration guar solutions, in the entangled regime, yielded different Giesekus fluid parameters for extension to those for simple shear. The extensional data for all concentrations of both gums collapsed to a common functional form, similar to that reported for cake batters[2]; the limits of the new filament thinning expression provide insight into this behaviour.

Keywords Concentration regimes · Extensional · rheology · Guar gum · Giesekus fluid · κ/ι-hybrid carrageenan gum · Shear rheology · Trouton ratio

M.D. Torres
Department of Chemical Engineering and Biotechnology, New Museums Site, University of Cambridge, Pembroke St, Cambridge, CB2 3RA, UK.
Department of Chemical Engineering, University of Santiago de Compostela, Lope Gómez de Marzoa St, Santiago de Compostela, E-15782, Spain.

B. Hallmark (✉)
Department of Chemical Engineering and Biotechnology, New Museums Site, University of Cambridge, Pembroke St, Cambridge, CB2 3RA, UK.
e-mail address: bh206@cam.ac.uk

L. Hilliou
Institute for Polymers and Composites/I3N, University of Minho, Campus de Azurém, 4800-058, Guimarães, Portugal.

D.I. Wilson
Department of Chemical Engineering and Biotechnology, New Museums Site, University of Cambridge, Pembroke St, Cambridge, CB2 3RA, UK.

Introduction

Many liquid-based foods exhibit complex rheological behaviour as a result of their multi-phase nature; examples include emulsions (liquid-liquid), dense suspensions (solid-liquid), polymer solutions, bubbly liquids and foams (both gas-liquid). The presence of a long-chain polymer or units of dispersed phase gives rise to a wide range of microstructures and deformation behaviours[1] that are desired in the product. The use of such materials is increasing, both in the design and formulation of new products and in supporting the replacement of traditional components such as fat and sugars in existing formulations.

Rheological testing is regularly employed to establish and quantify the deformation behaviour of food materials for materials characterisation and quality control purposes. It is also required for process engineering studies of food systems, where rheological measurements are allied with computational fluid dynamics (CFD) simulations of equipment in the design of new equipment and/or to confirm whether a new formulation can be processed on an existing multi-product line. Identification of the appropriate constitutive equation, and its associated parameters, is a critical step in this process. Food processing devices, such as filling nozzles and mixers, impose a mixture of linear and extensional shear on the material [2]and it is important that the constitutive equation used in the CFD calculations represents both modes of deformation properly.

Whereas devices for measuring shear viscosity have been available for a long time, commercial instruments for measuring extensional viscosities accurately and independently of shear contributions are relatively new. Extensional rheometers, such as the CaBER, the FiSER and the Cambridge Trimaster monitor the necking of extensionally-strained fluid filaments as a function of time, which allows rheological parameters to be calculated[3]. In the absence of direct measurements, CFD calculations have had to make assumptions about the relationship between extensional and shear flow behaviour, such as the magnitude of the Trouton ratio, Tr, which is the ratio of the extensional and shear viscosities at a given shear rate[4]. For a Newtonian fluid in uniaxial extension, $Tr = 3^4$. The value

of *Tr* is rarely known *a priori* for complex foods as these are usually non-Newtonian and the microstructural features that give rise to non-Newtonian behaviour will give rise to different dependencies on shear rate[1]. It is therefore important to establish whether there exist any cases of non-Newtonian behaviour which fit a non-Newtonian constitutive equation for both linear and extensional shear behaviour, so that measurements of one deformation mode can be used to predict the other with reasonable confidence, thereby reducing the amount of rheological testing.

This paper demonstrates that the Giesekus constitutive equation [5], which was originally developed to describe the shear behaviour of polymer solutions, gives a very good description of the shear and extensional rheology of aqueous guar gum and κ/ι-hybrid carrageenan gum solutions. One of the attractive features of the Giesekus equation is that it is available as standard in many commercial CFD software packages.

Guar gum is a galactomannan and one of the most cost effective natural neutral hydrocolloids due to its ready availability and ease of manufacture by extraction from *Cyamopsistetragonolobus* seeds. This long-chain polysaccharide biopolymer is highly polydisperse, has a semi flexible random coil conformation composed of a linear mannan backbone bearing side chains of a single galactose unit, and contains a mannose to galactose ratio of ~1.6-1.8:1. Guar gum is widely used in food and other applications as a thickener and rheology modifier. Aqueous solutions are shear thinning, and several studies [6–9] have demonstrated that its non linear shear rheology can be described very well by the Cross model [10]. The Cross model, however, is a generalised Newtonian model and hence does not provide an *a priori* estimate of extensional behaviour.

Carrageenans are natural linear polysaccharides extracted from red seaweeds (*Gigartinales, Rhodophyta*) and are extensively used as thickeners, gelling, texturing, suspending or stabilising agents[11]. Most carrageenophyte seaweeds produce κ/ι-hybrid carrageenans, and alternative algal resources for carrageenan production are needed to cope with the steadily increasing demand for food

texturing agents[11]. They are natural polyelectrolyte copolymers comprising blocks of κ or ι-carrageenan disaccharide units randomly distributed along the chain, together with minor amounts of non-gelling disaccharide units (biological precursors). The relative amount of κ or ι-depends on the plant biology and the biopolymer extraction procedure. The chemical structure of κ/ι-hybrid carrageenans has a direct impact on its gel properties as reported recently [12–14].

The extensional rheology of guar gum solutions has been studied widely[8,15,16], whereas there are no studies to date of aqueous κ/ι-hybrid carrageenan solutions. Bourbon *et a*l. employed a CaBER device to study a narrow range of guar gum concentrations (0.39-0.97 g/L) and compared their results with FENE constitutive models. We have recently presented measurements [1]of the extensional rheology of guar gum solutions obtained using the Cambridge Trimaster filament stretching device [17] over a wider range of concentrations (1-20 g/L), crossing the transition from the semi-dilute to the entangled regime. It will be shown that the Giesekus equation provides a good description of both linear and extensional shear behaviour of both these data sets and new sets obtained for κ/ι-hybrid carrageenan solutions.

The Giesekus model has been widely used to describe the shear response of solutions of synthetic polymers [18,19]. It has received little attention in the literature on food polymer solutions, even though it is able to account for the both the low and high shear rate plateau viscosities and the shear-thinning behaviour reported for many viscous food liquids. It has also been used to describe the extensional viscosity of synthetic polymers [3,20,21]. Anna and co-workers [3] fitted a multi-mode Giesekus model to data obtained from filament stretching of Boger fluids consisting of high molecular weight polystyrene dissolved in styrene oil: this required the solution of a set of coupled ordinary differential equations. This paper presents the derivation of a simple analytical expression that predicts the time-dependent viscoelastic filament thinning of a single-mode Giesekus fluid. This is found to give a good description of the experimental data obtained for the guar gum and κ/ι-hybrid carrageenan gum solutions. We are not aware of this result being presented previously elsewhere. It allows the

extensional behaviour to be compared with that expected from (linear) shear measurements. The ability to predict extensional behaviour from shear flow measurements is tested and shown to depend on whether the solution is semi-dilute and unentangled or whether the solution exists in the entangled regime.

Experimental

Sample preparation

Commercial guar gum was supplied by Sigma-Aldrich (batch no. 041M0058V, India). Theκ/ι-hybrid carrageenan gum was extracted from *M. stellatus* seaweed using the method described by Hilliou and co-workers [13]Aqueous solutions of guar gum (reported by Torres and co-workers[1])and κ/ι-hybrid carrageenan gum over a wide range of concentrations (1-20 g/L) were prepared following procedures established in the literature[7,12]. The guar gum was dispersed in tap water by stirring at 1400 rpm overnight on a magnetic hotplate stirrer (VMS-C4 Advanced, VWR, UK) at room temperature, between 19 °C and 21 °C, to ensure complete hydration of the gums. The aqueous κ/ι-hybrid carrageenan gum solutions were prepared by dissolving the gum in NaCl 0.1 M solutions, in order to fix the ionic strength. Some air was incorporated into the solution during stirring and deaerated samples of the continuous phase were obtained by centrifugation at 2250 rpm (500 *g*) for 5 min. All samples were, at minimum, duplicated.

Rheology measurements

Steady shear measurements were performed on a Bohlin CVO120HR controlled-stress rheometer (Malvern Instruments, Malvern, UK) using sand-blasted parallel plates (25 mm diameter and 1 mm gap) to prevent wall slippage. The normal force generated by the flow between plates was also measured. Measurements of axial thrust were used to estimate the normal stress difference, N_1–N_2[4]; calibration of this device indicated that reliable axial thrust data could be acquired for thrusts greater than 9.8×10^{-3} N. Samples were loaded carefully to ensure minimal structural damage, and held at rest for 5 min before testing to allow stress relaxation and temperature equilibration. A thin film of a

Newtonian silicone oil (viscosity 1 Pa s) was applied to the exposed sample edges to prevent evaporation. All measurements were made under isothermal conditions (20 ºC) and, at minimum, duplicated.

Extensional measurements were investigated using the Cambridge Trimaster, a high-speed filament stretch and break-up device [17]. The apparatus consists of two cylindrical 1.2 mm diameter stainless steel stubs which are moved vertically apart at speed with high spatial precision. Measurements reported here featured an initial gap spacing of 0.6 mm, final gap spacing of 1.5 mm, and piston separation speed of 75 mm s^{-1}. The initial filament diameter, D_1, was measured once the stainless steel stubs had reached their final position; this parameter was strongly dependent on the fluid properties and was often slightly different for each experiment. The filament stretching and thinning profiles were monitored using a high speed camera (Photron Fastcam 1024 PCI) which allows the diameter of the filament midpoint to be measured to within 1 μm at a rate of 6000 frames per second. The device did not feature a force transducer so separating forces were not recorded. All experiments were performed at least in duplicate in an air-conditioned room at 20 °C. Error bars corresponding to experiment variation of repeated steady shear and extensional tests are plotted where the measurement uncertainty was greater than the symbol size. Further information about the used protocols can be found in a previous publication [1].

Theory

Giesekus model for shear behaviour

The total stress in a fluid, $\boldsymbol{\sigma}$, is written as

$$\boldsymbol{\sigma} = -p\mathbf{I} + \boldsymbol{\tau} \quad (1),$$

where p is the hydrostatic pressure and $\mathbf{I}$ the identity tensor. In the Giesekus constitutive equation [5,22], the shear stress, $\boldsymbol{\tau}$, is modelled as

$$\frac{\boldsymbol{\tau}}{\lambda} + \frac{\partial \boldsymbol{\tau}}{\partial t} + \mathbf{v}\nabla\boldsymbol{\tau} - \left(\left(\nabla\mathbf{v}\right)^{\mathrm{T}}\boldsymbol{\tau} + \boldsymbol{\tau}\left(\nabla\mathbf{v}\right)\right) = \frac{\eta_0}{\lambda}\dot{\boldsymbol{\gamma}} - \frac{a}{\eta_0}\boldsymbol{\tau}\cdot\boldsymbol{\tau}$$

154 (2),

155 where **v** is the velocity vector, η_o is the zero shear (Newtonian) viscosity, t is time, λ is the
156 characteristic relaxation time and a is the mobility parameter; the mobility parameter describes the
157 anisotropy of hydrodynamic drag and Brownian motion on the polymer molecule [23]. The rate-of-
158 strain-tensor, $\dot{\boldsymbol{\gamma}}$, is

159

160 $$\dot{\boldsymbol{\gamma}} = \left(\nabla \mathbf{v}\right) + \left(\nabla \mathbf{v}\right)^{\mathrm{T}}$$

161 (3).

162 Expressions that describe the shear rate dependence of the shear viscosity as a function of shear rate
163 for a single-mode Giesekus fluid have been presented in the literature [5]. These expressions have been
164 successfully applied to describe the flow curve of aqueous solutions of rod-like micelles for the
165 surfactant system cetyltrimethylammonium[20], and are used here to describe the steady, one-
166 dimensional, shear response of guar gum and κ/ι-hybrid carrageenan gum solutions of varying
167 concentrations. In summary,

168 $$\eta\left(\dot{\gamma}\right) = \frac{\eta_0\left(1-n_2\right)}{1+\left(1-2a\right)n_2}$$

169 (4).

170 Here the dimensionless terms n_2 and Λ are given by

171 $$n_2 = \frac{1-\Lambda}{1+\left(1-2a\right)\Lambda}$$

172 (5),

173 $$\Lambda = \sqrt{\frac{\sqrt{1+16a\left(1-a\right)\lambda^2\dot{\gamma}^2}-1}{8a\left(1-a\right)\lambda^2\dot{\gamma}^2}}$$

174 (6).

175 For steady shear at steady shear rate, Eq. (2) implies that first normal stress difference, N_1, is of the
176 form[24,25]

177 $$N_1 = 2\lambda\eta_0 \frac{n_2(1-an_2)}{\lambda^2 a(1-n_2)}$$

178 (7).

179 Over some concentration ranges, the second normal stress difference, N_2, has been observed to
180 be$N_2 \sim -N_1/10$[26]. For this work, however, the analytical form of the second normal stress difference
181 for a Giesekus fluid was used[25]

182 $$N_2 = \frac{-aN_1}{2} \frac{(1-n_2)}{(1-an_2)}$$

183 (8).

184 Equations (7) and (8) were then used to estimate the magnitude of the stress difference, N_1 - N_2,
185 measured in the steady shear experiments.

186

187 Derivation of a simple expression for the extensional behaviour of a Giesekus fluid

188 The derivation of the extensional thinning of a filament of cylindrical thread of a Giesekus fluid
189 follows similar lines to that of Entov and Hinch[27], in their analysis of the filament breakup of dilute
190 polymer solutions using a finitely extensible nonlinear elastic (FENE) model [28]. Other authors, notably
191 the McKinley group at MIT, have derived simple expressions that describe viscoelastic filament
192 breakup using the FENE-P model [3] along with models involving coupled ordinary differential
193 equations that describe the filament breakup of Giesekus fluids [29]. This section presents the derivation
194 of a simple expression that predicts time-dependent viscoelastic filament thinning of a single-mode
195 Giesekus fluid.

196

197 The first simplification made is to assume that extensional deformations only occur in the axial and
198 radial directions within the liquid filament, and that the divergence of the extra stress tensor is zero.
199 This allows Equation (2) to be simplified to a pair of ordinary differential equations, which are a
200 function of the axial and radial components of the stress within the filament, *viz*.

201 $$\frac{\tau_{zz}}{\lambda} + \frac{\partial \tau_{zz}}{\partial t} - \tau_{zz}\dot{\gamma}_{zz} = \frac{\eta_0}{\lambda}\dot{\gamma}_{zz} - \frac{a}{\eta_0}\tau_{zz}^2$$

202 (9),

203 $$\frac{\tau_{rr}}{\lambda}+\frac{\partial \tau_{rr}}{\partial t}-\tau_{rr}\dot{\gamma}_{rr}=\frac{\eta_0}{\lambda}\dot{\gamma}_{rr}-\frac{a}{\eta_0}\tau_{rr}^{\ 2}$$

204 (10).

205 The boundary conditions on the liquid filament assume that any end effects, where the liquid filament
206 may contact a surface, are negligible resulting in zero axial stress. This assumption is commonly used
207 when deriving expressions for extensional thinning[30] but strictly speaking requires experimental
208 validation. Alternative assumptions can include an exponential increase in normal stress for
209 viscoelastic fluids[31]. Furthermore, it is assumed that surface tension, α, alone is responsible for the
210 radial stress that causes the filament to thin, with the radial stress being assumed to be equal to the
211 Laplace pressure. These boundary conditions can be derived from Equation (1) and give

212 $$\sigma_{zz}=0=-p+\tau_{zz}$$

213 (11),

214 $$\sigma_{rr}=-p+\tau_{rr}=-\frac{2\alpha}{D}$$

215 (12).

216 Equation (11) allows the unknown hydrostatic pressure, p, to be calculated, which can then be
217 substituted into Equation (12); this leads to an expression that relates the radial and axial components
218 of the stress to the surface tension and to the filament diameter. It is now assumed that the axial
219 extensional stress is the dominant stress in the problem giving the following relationship between this
220 stress, the surface tension and filament diameter, D.

221 $$\tau_{zz}\approx\frac{2\alpha}{D}$$

222 (13).

223 In order to calculate the variation of the filament diameter as a function of time, the strain rate in the
224 radial direction can be related to the change in velocity in the radial direction velocity, *i.e.*

225 $$\dot{\gamma}_{rr}=2\frac{\partial \mathrm{v}_r}{\partial r}$$

226 (14).

227 This, in turn, can then be related to the filament diameter, giving

228 $$\dot{\gamma}_{rr} = 2\frac{\partial}{\partial r}\left(\frac{\partial r}{\partial t}\right) = \frac{4\partial}{\partial D}\left(\frac{1}{2}\frac{\partial D}{\partial t}\right) = 2\frac{\partial^2 D}{\partial D \partial t}$$

229 (15).

230 Integration of Equation (15) with respect to the filament diameter yields a simple ordinary differential

231 equation in terms of radial direction shear rate;

232 $$\frac{\mathrm{d}D}{\mathrm{d}t} = -\frac{\dot{\gamma}_{zz}}{4}D$$

233 (16).

234 The radial and axial components of the strain rate can then be related by remembering that the

235 deformation is a uniaxial extension. The expressions for axial extension rate, Equation (16), and

236 approximate axial tensile stress, Equation (13), can now be substituted into the axial component of the

237 Giesekus expression, which was shown in Equation (9). The resulting expression is

238 $$\frac{2\alpha}{D\lambda} + 2\alpha\frac{\mathrm{d}}{\mathrm{d}t}\left(\frac{1}{D}\right) + \frac{8\alpha}{D^2}\frac{\mathrm{d}D}{\mathrm{d}t} = \frac{-4\eta_0}{D\lambda}\frac{\mathrm{d}D}{\mathrm{d}t} - \frac{4a\alpha^2}{\eta_0 D^2}$$

239 (17).

240 Some manipulation and reorganisation of the terms in Equation (17) result in a single, non-linear,

241 ordinary differential equation that relates the rate of change of filament diameter to the physical

242 properties of the fluid:

243 $$\frac{\mathrm{d}D}{\mathrm{d}t} = \frac{-\alpha}{\eta_0}\left(\frac{\eta_0 D + 2a\lambda\alpha}{2\eta_0 D + 3\alpha\lambda}\right)$$

244 (18).

245 Integration of Equation (18), subject to the initial condition that at $t = 0$ the initial filament diameter

246 isD_1, yields

247 $$\frac{\alpha\lambda(3-4a)}{\eta_0}\ln\left(\frac{\eta_0 D + 2a\lambda\alpha}{\eta_0 D_1 + 2a\lambda\alpha}\right) + 2(D - D_1) = \frac{-\alpha t}{\eta_0}$$

248 (19).

An analogous derivation for an upper convected Maxwell (UCM) fluid[32] makes the assumption that viscous stresses are negligibly small when compared to elastic stresses. For the condition that both $a = 0$ and $\eta_0 = 0$, Equation (19) simplifies to the expected UCM result for extensional filament thinning where $D/D_1 = \exp\left(-t/3\lambda\right)$.Equation (19) relates the filament diameter implicitly to time, making it more straightforward to calculate the variation in time as a function of a given filament diameter, rather than *vice versa*. Equation (19) can also be expressed in non-dimensional form as

$$(4a-3)\ln\left(\frac{\left(D/D_1\right)+2a\lambda\alpha/D_1\eta_0}{1+2a\lambda\alpha/D_1\eta_0}\right)-\frac{2\eta_0 D_1}{\alpha\lambda}\left(D/D_1-1\right)=\frac{t}{\lambda} \quad (20).$$

Equation (20) highlights that there are two contributions to the characteristic timescale for the thinning of the liquid thread. The first term on the left hand side contains the Giesekus mobility parameter, which relates to the anisotropic relaxation of the polymer chains. The second term, which would also arise from the Upper Convected Maxwell constitutive equation, contains terms that relate to the longest relaxation time, zero shear rate viscosity and surface tension alone.

In the absence of direct measurements of extensional force (as in the case of the Trimaster device used to collect the extensional data presented here), it is possible to estimate the extensional viscosity, η_E, of a fluid undergoing a uniaxial extension using [17]:

$$\eta_E = (2X-1)\frac{-\alpha}{dD/dt} \quad (21).$$

In this expression, X is a coefficient that accounts for the deviation of the filament shape from a uniform cylinder due to inertia and gravity; in other studies this has been assumed to be roughly 0.7 [17,33]. Combining Equation (18) with Equation (21) yields the following estimate of the extensional viscosity of a Giesekus fluid:

$$\eta_E = \eta_0 (2X - 1) \frac{3 + 2\eta_0 D/\alpha\lambda}{2a + \eta_0 D/\alpha\lambda} \quad (22).$$

Equation (22) allows the extensional viscosity to be estimated relatively simply for a Giesekus fluid. Other methods[34] of estimating the extensional viscosity for FENE fluids are described in the literature; these involve interpolation between the asymptotic and perturbation solutions that respectively describe the limiting cases of extensional viscosity a large and small extension rates.

Statistical analysis

The parameters of the models considered were determined from the experimental data with a one-factor analysis of variance (ANOVA) using PASW Statistics (v.18, IBMSPSS Statistics, New York, USA). When the analysis of variance indicated differences among means, a Scheffé test was performed to differentiate means with 95% confidence ($p < 0.05$).

Results and discussion

Concentration regimes

Both the guar gum and carrageenan solutions were found to be shear thinning and highly viscoelastic, with each property being strongly dependent on concentration. The effect of concentration on the guar gum solutions was investigated in our previous paper [1] and the results are summarised here alongside new results for the κ/ι-hybrid carrageenan solutions.

The dynamic response of the guar gum solutions to oscillatory shear testing indicated a transition from being predominantly viscous, at concentrations below ~5 g/L to exhibiting a significant elastic response at higher concentrations. This transition was not observed in the κ/ι-hybrid carrageenan gum solutions, which indicated predominantly viscous behaviour over the frequency range investigated (data not reported) for all concentrations tested. This suggested that the carrageenan solutions were in the semi-dilute regime, while the higher concentrations of guar gum were subjected to significant entanglements.

299

300 Another observation suggesting that the threshold of the entangled regime for the guar gum solutions
301 lay near 10 g/L was that the measured surface tension deviated from the Szyszkowski equation [35] at 10
302 g/L, indicating that the solution was exhibiting behaviour analogous to that associated with critical
303 aggregation concentration [36]. This is consistent with other reported studies of guar sum solutions
304 [37,38].In contrast, the concentration dependence of surface tension of κ/ι-hybrid carrageenan gum
305 solutions was satisfactorily fitted to the Szyszkowski equation[35] over the whole concentration range
306 studied (see Appendix, Figure A.1).

307

308 In the semi-dilute coil overlap region, the reduced viscosity, η_{red}, is expected to follow the Martin
309 equation[39], *viz*:

310
$$\frac{\eta_0 - \eta_s}{c\,\eta_s} = \eta_{red} = [\eta]\exp\left(k[\eta]c\right)$$

311 (23)

312 where η_s is the solvent viscosity, c the solution mass concentration, $[\eta]$ the intrinsic viscosity and k the
313 Huggins parameter. In this region the coil overlap parameter, $c[\eta]$, is expected to lie between $1 < c[\eta]$
314 <10. The zero shear rate viscosity values were used to estimate η_{red} and are plotted against c in Figure
315 1(*a*). The guar gum data fit Equation (23) reasonably for $c \leq 5$ g/L but deviate strongly from the trend
316 at higher concentrations. Linear regression yielded $[\eta]$ = 1.09±0.02 L/g and k = 0.84±0.07, which
317 compare favourably with the values for similar gums[40], namely $[\eta]$= 1.06L/g, and k = 1.07 at 24°C
318 and 0.73 at 45°C. Other studies of guar gum and similar materials [4,7,8] have reported similar behaviour.
319 The κ/ι-hybrid carrageenan gum data showed a good fit to Equation (23) over the whole concentration
320 range studied, giving $[\eta]$ = 1.05±0.01 L/g and k = 0.34±0.03. The $[\eta]$ values are consistent with those
321 previously reported for κ/ι-hybrid carrageenan gum solutions [41]. Values of $k < 0.5$ indicate systems
322 where the solvent-polymer interactions are favoured over polymer-polymer interactions[39,40]. Namely,
323 the polyelectrolyte nature of the κ/ι-hybrid carrageenan gum is mirrored in Figure 1(*b*). The double

logarithmic plot confirms the expected power law behaviour for polyelectrolytes polymers approaching the theoretical one, $\eta_0 / \eta_s \sim k' c^{15/4}$, for semi dilute-entangled regime of polyelectrolyte solutions[42], with k' values of 0.12.

Shear thinning behaviour

The shear flow data for both gums gave a good fit to the Cross model [1]for the guar gum data, carrageenan results provided in the Appendix, Figure A.2, but this model does not provide insight into extensional behaviour. Figure 2(*a*) shows that the Giesekus model (Equation (4)) gives a good description ($R^2 > 0.988$) of the shear flow data for guar gum solutions in the semi-dilute regime (c = 1-5 g/L). There is an increasingly poorer fit in the entangled regime as the concentration increases (≥ 10 g/L). In contrast, Figure 2(*b*) shows that theκ/ι-hybrid carrageenan gum solutions exhibited Giesekus-fluid behaviour over the whole concentration range studied.

Equation (4) has three adjustable parameters: the zero shear rate viscosity, the Giesekus mobility parameter and the relaxation time; η_0 was taken from the experimental data at the lowest shear rate studied, 0.01 s^{-1}. The remaining two parameters, a and λ, were fitted to the experimental data by a least squares algorithm and the results are presented in Figure 3. Several workers[43,44] have reported that although the theoretical range of the mobility parameter is $0<a<1$, physically realistic solutions are only obtained for the range $0<a<0.5$. An upper limit of 0.5 was hence used here.

The fit in Figure 2(*a*) obtained for higher concentrations for guar gum solutions is arguably less good than at lower concentrations, due to the limitation of having a single relaxation time. Figure 2(*a*) also shows a marked increased in apparent viscosity with concentration. The highest concentration in these tests, 20 g/L, corresponds to a polymer volume fraction of 0.055 and Figure (*a*) shows an increase of six orders of magnitude in η_0 for a 20× increase in guar gum concentration. A similar trend is seen with theκ/ι-hybrid carrageenan, Figure 2(*b*), albeit with a smaller increase (four orders of magnitude) over the concentration range.

Figure 3 shows that all three Giesekus parameters exhibited a strong dependency on concentration in the semi-dilute regime. The plots shows that these data could be described reasonably well by power law relationships of the form

$$f(c) = K^* c^n \tag{24}$$

with the values of the prefactor, K^*, and power law index, n, obtained by regression presented in Table 2.Above a critical concentration of 10 g/L guar gum solutions did not fit these trends, with η_0 and λ exceeding the values obtained by extrapolation, and a reaching the upper limit of 0.5.

In the semi-dilute region η_0 and a exhibit similar sensitivity to c, with $n \sim 3$ for guar gum solutions and $n \sim 4$ for κ/ι-hybrid carrageenan gum solutions, whilst the relaxation time is less sensitive to c, with $n \sim 2$ and 3, respectively. These values can be compared with those expected from scaling theories, but this was not pursued here as only one sample of each gum was studied here. More detailed studies with gums of different molecular weight should follow. These results suggest that the Giesekus parameters in the semi-dilute regime can be estimated for engineering purposes from knowledge of the solution concentration alone.

The normal stress difference data, N_1-N_2, presented in Figure 4 indicate that κ/ι-hybrid carrageenan gum solutions generate smaller elastic responses than those featured in guar gum solutions. The aqueous guar gum solutions show appreciable elastic responses at high shear rates. N_1-$N_2$for guar gum solutions at 2 g/L was practically negligible, in that the measured thrust lay within the noise floor for the rheometer whereas for c = 20 g/L N_1-N_2 increased rapidly at shear rates above 1 s^{-1}. The shear rate at which N_1-N_2 increased noticeably was smaller at higher concentrations. Furthermore, the shear rate at which N_1-N_2 increased corresponds to the onset of noticeable shear-thinning in Figure 2. The N_1-N_2values of κ/ι-hybrid carrageenan gum solutions approached a common value at high shear rates.

Figure 4 also shows that the normal stress differences predicted by Equations (7) and (8), gives very good agreement for the guar gum solutions in the semi-dilute regime and all the κ/ι-hybrid carrageenan gum solutions tested. It should be noted that the lines in Figure 4 are computed using the parameters obtained from fitting the Giesekus model (Equation (4)) to the shear stress data, not the measured normal force. The values of the model parameters η_0, λ and a are those given in Table 1.

Filament stretching behaviour

Plots of filament stretching data such as those in Figure 5 exhibit features observed in other studies, namely an initially linear decrease in ln D/D_1 with time followed a steep reduction in D/D_1 as the filament approaches rupture at time t_F.

The guar gum and κ/ι-hybrid carrageenan gum data were compared with existing models for extension of single- and multi-mode FENE materials [3,27] and gave a poor fit. In contrast, the single-mode Giesekus model, Equation (2), gives good agreement for both the guar gum solutions at lower concentrations and all the κ/ι-hybrid carrageenan gum solutions tested. It should be emphasised that lines in Figure 5are computed with Equation (19), using the parameters obtained from fitting the Giesekus model (Equation (4)) to the data from shear experiments (see Figure 2): the values of the model parameters η_0, λ and a are those given in Table 1. The values of the liquid-air surface tension, α,in Equation (19)for guar gum are those previously reported[1], while the values for the κ/ι-hybrid carrageenan solutions were determined for this study using the same protocol (see Appendix, Figure A.1).

The agreement between the experimental data and the prediction for κ/ι-hybrid carrageenan gum solutions prepared at 5 g/L (Figure 5(*a*)) and for the semi-dilute guar gum solutions prepared at 1 g/L and 2 g/L (Figure 5(*b*)) is excellent (R^2> 0.990). The filament rupture time, when D/D_1 approaches zero rapidly, is predicted quite well for the 5 g/L case but the evolution in D/D_1 prior to this deviates noticeably from the model. These results indicate that Equation (19) is able to describe the extensional

behaviour of the semi-dilute guar gum solutions with parameters obtained from shear flow tests. The converse is expected to follow, that shear flow behaviour could be predicted using extensional tests. Extensional tests have the advantage of requiring very small volumes of liquids, however shear flow devices are able to assess the influence of phenomena such as wall slip; this could not be predicted from extensional testing alone.

Figure 5(*c*) shows progressively less good agreement between the experimental data and the model predictions as guar gum concentration increases within the entangled regime. At 10 g/L, where entanglement is apparent, and there is an associated increase in the magnitude of the elastic response [1], Equation (19) does not give a good prediction of the extensional behaviour when the parameters obtained from Equation (4) are used. The fit is even poorer with higher concentrations.

The derivation of Equation (19) involves the assumption that the axial stress dominates over the radial stress; guar gum solutions that have a significant elastic response will also have significant first normal stress differences[1], possibly invalidating this assumption. This may be the cause of the failure of Equation (19) to fit the data at high concentrations. It may also be the case, however, that the constitutive model needs to be revised in order to capture the phenomena associated with the extension of the guar gum solutions, such as using a multi-mode formulation. The approach taken here was to allow the mobility parameter, a, and relaxation time, λ, to differ from the values obtained from the shear flow data in Figure 2. D_1, η_0, η_∞ and α are not altered. Figure 6 shows that Equation (19) gives a very good fit ($R^2 > 0.992$) to the data at 5 g/L and 10 g/L if the mobility parameter and relaxation time are allowed to differ from those obtained from fitting to the linear shear data in Figure 2(*a*). The revised values of a and λ are reported alongside those obtained from shear flow testing in Table 3. The revised values of a are smaller, 0.63 for 5 g/L and 0.92 for 10 g/L, while the relaxation parameter decreases by over an order of magnitude to give similar values (29ms for 5 g/L *cf*. 23ms for 10 g/L). These results are consistent with those previously reported for a wormlike micellar solution[45] and for different commercial thickeners[46].

Comparing the guar gum shear data in Figure 2(*a*) with the extensional data in Figure 6, it can be seen that the extensional response becomes substantially independent of solution concentration at $c > \sim 10$ g/L. In contrast, the shear flow apparent viscosity increases by approximately two orders of magnitude between c = 10 g/L and 20 g/L. These results indicate that different physical mechanisms govern the deformation response and it is unlikely that a simple, single-mode, model will cease to describe both behaviours. A multi-mode formulation is likely to be needed for the entangled regime.

Time-concentration superposition and rupture time

An alternative means of describing the extensional behaviour of guar gum and κ/ι-hybrid carrageenan gum solutions, seemingly independently of solution regime, is to use time-concentration superposition as previously reported[1,2]. In this approach the non-dimensional filament diameter is plotted against normalised time, where time is normalised by the filament rupture time. The plots demonstrate that κ/ι-hybrid carrageenan gum solutions (Figure 7(*a*)) and guar gum solutions in both the semi-dilute and entangled regime (Figure 7(*b*))collapse onto a single master curve; analogous behaviour has been reported for other biopolymeric solutions, such as cellulose [47], where self-similar filament thinning behaviour is observed when the time is normalised by the polymer relaxation time. The parameter in this semi-empirical model is the filament rupture time, which increases monotonically with gum concentration and is less sensitive to concentration at higher values: t_F approaches an asymptote in the entangled regime, in a similar fashion to the mobility parameter (see Figure 3(*b*)). Figure 8 shows that the two parameters, t_F and a, are closely correlated.

Insight into this behaviour can be gained from examining Equation (20). As the non-dimensional filament diameter, D/D_1, tends to zero, the time, t, tends to the filament rupture time, t_F, *viz*:

$$\left(4a-3\right)\ln\left(\frac{2aA}{1+2aA}\right)+\frac{2}{A}=\frac{t_F}{\lambda} \qquad (25),$$

where

$$A = \frac{\lambda \alpha}{\eta_0 D_1} \tag{26}$$

Close examination of Equation (25) reveals that the filament rupture time, t_F, actually decreases with increasing mobility parameter but increases with increasing zero shear rate viscosity. The trend shown in Figure 8 can be explained by the fact that both the mobility parameter and zero shear rate viscosity increase with increasing solution concentration; in this case the increase in t_F due to the increasing solution viscosity outweighs the decrease in t_F due to increasing mobility parameter.

This result suggests that the filament rupture time can be estimated from the shear flow tests. This is tested by evaluating the left hand side (LHS) of Equation (25), using the parameters listed in Table 1, and comparing the result with the t_F values divided by the relaxation time. One could also multiply the LHS by λ to give a comparison of estimated against experimental times. Figure 9 shows that the equality is obeyed for the κ/ι-hybrid carrageenan gum solutions over the entire concentration range investigated, and the guar gum solutions in the semi-dilute regime. The predictive relationship does not hold for the guar gum solutions in the entangled regime.

Equation (25) also provides a prediction of filament rupture time if the product aA is large so that the argument of the log term approaches unity. This gives:

$$t_F \approx \frac{2\lambda}{A} = \frac{2\eta_0 D_0}{\alpha} \tag{27}$$

Substitution of this result into Equation (20) yields

$$(4a-3)\ln\left(\frac{\frac{t_F}{\lambda}\left(\frac{D}{D_1}\right)+4a}{\frac{t_F}{\lambda}+4a}\right)-\frac{t_F}{\lambda}\left(\frac{D}{D_1}\right)=\frac{t_F}{\lambda}\left(\frac{t}{t_F}-1\right)$$

(28)

Here, the non-dimensional filament diameter appears scaled by the ratio of the filament rupture time to the relaxation time. This scaling gives insight into why time-concentration superposition gives the master curve in Figure 8. It is also instructive to note that the steady-state extensional viscosity for a Giesekus fluid[25] is given by $\eta_E \approx 2\eta_0/a$ which explains the presence of this grouping in Equations (27) and (29).

For the case where A is large and the mobility parameter $a = 0.5$ (the upper limit suggested in the literature [43,44]), it can be shown that Equation (20) predicts a rupture time longer than that given by Equation (27), namely:

$$t_F \approx \frac{3\lambda}{A} = \frac{3\eta_0 D_0}{\alpha} \quad (29).$$

For the guar gum solutions tested in the entangled regime, the condition of aA being large is not met, hence Equation (27) could not be used to predict the filament rupture time. With c = 10 g/L, however, the mobility parameter a = 0.5 and the product aA = 28.5; Equation (29) predicts a rupture time of 125ms which compares reasonably with the experimental value of 111ms.

Trouton ratio

The Troutonratio[48] quantifies the relationship between the shear and extensional viscosities. For a uniaxial extensional flow, the Trouton ratio, Tr, is given by

$$\mathrm{Tr} = \frac{\eta_E\left(\dot{\varepsilon}\right)}{\eta\left(\sqrt{3}\dot{\varepsilon}\right)} \quad (30),$$

where the extensional and shear viscosities, η_E and η respectively, are evaluated at the Hencky strain rate, $\dot{\varepsilon}$, and shear rate equivalent to $\sqrt{3}\dot{\varepsilon}$. The Hencky strain for cylindrical filament thinning can be evaluated from[17]

$$\varepsilon = 2\ln\left(\frac{D_0}{D(t)}\right) \quad (31).$$

The *Tr* values for the guar gum solutions in the semi-dilute guar gum regime, evaluated at different Hencky strains, are compared with the Giesekus model predictions (calculated using η_E from Equation (21) and η from Equation (4)) in Figure 10.The same comparison for κ/ι-hybrid carrageenan gum is shown in the Appendix, Figure A.3. *Tr* is always >3, the value expected for a Newtonian fluid, confirming that studies of the type presented here are required if these materials are to be simulated reliably. There is broad agreement, over four orders of magnitude, between the experimental values and the model predictions. Good quantitative agreement is again evident with small *c*, at the lower end of the semi-dilute regime, and greater deviation evident at the upper end of the semi-dilute regime for guar gum solutions. The qualitative trend is captured for both *c* = 5 g/L and 10 g/L, and the quantitative differences are close enough to give reasonable estimates. There is significant disagreement between the experimental values of *Tr* and the model predictions for the entangled regime for guar gum solutions, where *c* = 15 g/L and 20 g/L. The origin of this disagreement can be seen by examining the differences in the values of the mobility parameter and relaxation time according to whether the fitting was carried out with shear or extensional data; these are given for the upper end of the semi-dilute regime in Table 3. When making the transition to the entangled regime, the dynamics of the polymer solution are not sufficiently described by one characteristic timescale alone; both reputation dynamics and unentangled chain stretching are contributory factors. The single-mode formulation of the Giesekus fluid used in this work cannot capture both of these contributions, and is hence unable to predict the response of the fluid in the entangled regime. Good quantitative agreement was obtained for the κ/ι-hybrid carrageenan gum solutions (see Appendix, Figure A.3).

These results provide confidence in using the expressions developed here as a reasonable starting point to describe both the shear and extensional response of these gum solutions, and possibly other biomacromolecular materials, in the semi-dilute regime.

Conclusions

A simple expression is presented describing the extensional behaviour of a Giesekus fluid undergoing filament stretching. This expression, and one for simple shear reported previously by Giesekus[5], was used to analyse sets of shear and extensional rheological data reported for aqueous solutions of guar gum[1]and new experimental data obtained for κ/ι-hybrid carrageenan gum solutions at concentrations ranging from 1-20 g/L. The range of guar gum concentrations studied found to span the transition from the semi-dilute to entangled regime, based on measurements of the intrinsic viscosity and surface tension.

A single set of Giesekus parameters was found to provide a good quantitative description of both simple and extensional shear behaviour for guar gum solutions in the semi-dilute regime and all the κ/ι-hybrid carrageenan gum solutions. The parameters were dependent on gum concentration, and the Trouton ratio deviated strongly from the Newtonian value of 3. These findings indicate that the Giesekus model can be used to describe the rheology of these materials in CFD simulations. It also suggests that simple shear tests can be used to give a reliable estimate of their extensional behaviour.

At higher guar gum concentrations, both the simple and extensional shear behaviour gave poorer fits to the expressions for a single term Giesekus fluid. For solution concentrations towards the upper limit of the semi-dilute regime (c = 5 g/L and 10 g/L) the expressions still fitted the data well, but with separate mobility parameters and relaxation times for simple and extensional shear modes. This could be attributed to the effect of chain overlap on extension over simple shear. At the highest concentration studied the expressions did not describe the data sets well.

554 The filament thinning data sets all collapsed to a common curve for that material when presented in
555 terms of the fractional rupture time. The filament-thinning expression derived from the Giesekus
556 model provided insight into this behaviour.
557

558 ## Acknowledgements

559 The authors acknowledge financial support (POS-A/2012/116) for MDT from Xunta de Galicia's
560 Consellería de Cultura, Educación e OrdenaciónUniversitaria of Spain and the European Union's
561 European Social Fund. Helpful and insightful comments from the reviewers are also gratefully
562 acknowledged.
563

564 ## Nomenclature

565 ### Roman letters

A	Dimensionless group	-	N_1	First normal stress difference	Pa
a	Giesekus mobility parameter	-	N_2	Second normal stress difference	Pa
s_1	Szyszkowski fitting parameter	N/m	n	Power law exponent	
s_2	Szyszkowski fitting parameter	g/L	n_2	Parameter in shear expression	-
c	Solution concentration	g L^{-1}	p	Hydrostatic pressure	Pa
D	Filament diameter	m	r	Radial direction	m
D_0	Initial filament diameter	m	Tr	Trouton ratio	-
D_1	Initial filament diameter	m	t	Time	s
$\mathbf{I}$	Identity tensor	-	t_F	Filament rupture time	s
K^*	Power-law prefactor	various	$\mathbf{v}$	Velocity vector	m s^{-1}
k	Huggins parameter	-	v_r	Radial velocity	m s^{-1}
k_c	Time constant	s^{1-n}	X	Shape coefficient	-
k'	Proportionality constant	various			

566

567

568 **Greek letters**

α_0	Solvent surface tension	N m^{-1}	η_s	Solvent viscosity	Pa s
α	Surface tension	N m^{-1}	$[\eta]$	Intrinsic viscosity	L g^{-1}
$\dot{\varepsilon}$	Hencky strain rate	s^{-1}	Λ	Group used within shear	-
ε	Hencky strain	-	λ	Relaxation time	s
$\dot{\gamma}$	One dimensional shear rate	s^{-1}	$\boldsymbol{\sigma}$	Total stress tensor	Pa
$\dot{\gamma}_{rr}$	Radial-direction extensional rate	s^{-1}	σ_{rr}	Radial direction total stress	Pa
$\dot{\gamma}_{zz}$	Axial-direction extensional rate	s^{-1}	σ_{zz}	Axial direction total stress	Pa
$\dot{\boldsymbol{\gamma}}$	Rate-of-strain tensor	s^{-1}	$\boldsymbol{\tau}$	Extra stress tensor	Pa
η	Apparent shear viscosity	Pa s	τ_{rr}	Radial direction extensional	Pa
η_{app}	Apparent viscosity, Cross model	Pa s	τ_{zz}	Axial direction extensional stress	Pa
η_E	Extensional viscosity	Pa s			
η_0	Zero-shear-rate viscosity	Pa s			
η_{red}	Reduced viscosity	L g^{-1}			

569

References

1. Torres MD, Hallmark B, Wilson DI. Effect of concentration on shear and extensional rheology of guar gum solutions. *Food Hydrocolloids*. 2014;40:85-95.

2. Chesterton A, Meza B, Moggridge G, Sadd P, Wilson. Rheological characterisation of cake batters generated by planetary mixing: Elastic versus viscous effects. *Journal of Food Engineering*. 2011;105(2):332-342.

3. Anna SL, McKinley GH. Elasto-capillary thinning and breakup of model elastic liquids. *Journal of Rheology*. 2001;45(1):115.

4. Steffe J. *Rheological methods in food process engineering*. East Lansing: Freeman Press; 1996.

5. Giesekus H. A simple constitutive equation for polymer fluids based on the concept of deformation-dependent tensorial mobility. *Journal of Non-Newtonian Fluid Mechanics*. 1982;11:69-109.

6. Chenlo F, Moreira R, Pereira G, Silva C. Rheological modelling of binary and ternary systems of tragacanth, guar gum and methylcellulose in dilute range of concentration at different temperatures. *LWT-Food Science and TechnologyTechnology*. 2009;42:519-524.

7. Chenlo F, Moreira R, Silva C. Rheological properties of aqueous dispersions of tragacanth and guar gums at different concentrations. *Journal of Texture Studies*. 2010;41:396-415.

8. Bourbon A, Pinheiro A, Ribeiro C. Characterization of galactomannans extracted from seeds of Gleditsia triacanthos and Sophora japonica through shear and extensional rheology: *Food Hydrocolloids*. 2010;24(2-3):184-192.

9. Launay B, Cuvelier G, Martinez-Reyes S. Viscosity of locust bean, guar and xanthan gum solutions in the Newtonian domain. *Carbohydrate Polymers*. 1997;34:385-395.

10. Cross M. Rheology of non-Newtonian fluids: a new flow equation for pseudoplastic systems. *Journal of Colloid Science*. 1965;20:417-437.

11. Hilliou L, Larotonda FDS, Abreu M, Sereno AM, Gonçalves MP. The impact of seaweed life phase and postharvest sotarge duration on the chemical and rheological properties of hybrid carrageenans isolated from Portuguese Mastocarpus stellatus. *Carbohydrate Polymers*. 2012;87:2655-2663.

12. Souza HKS, Hilliou L, Bastos M, Gonçalves MP. Effect of molecular weight and chemical structure on thermal and rheological properties of gelling κ/ι-hybrid carrageenan solutions. *Carbohydrate Polymers*. 2011;85:429-438.

13. Hilliou L, Larotonda FDS, Abreu M, Ramos AM, Sereno AM, Gonçalves MP. Effect of extraction parameters on the chemical structure and gel properties of κ/ι-hybrid carrageenans obtained from Mastocarpus stellatus. *Biomolecular Engineering*. 2006;23:201-208.

14. Azevedo G, Hilliou L, Bernardo G, et al. Tailoring kappa/iota-hybrid carrageenan from Mastocarpus stellatus with desired gel quality through pre-extraction alkali treatment. *Food Hydrocolloids*. 2013;31:94-102.

15. Tatham J, Carrington S, Odell J, Gamboa A, Muller A, Saez A. Extensional behavior of hydroxypropyl guar solutions: Optical rheometry in opposed jets and flow through porous media. *Journal of Rheology*. 1995;39:961-986.

16. Duxenneuner M, Fischer P, Windhab E, Cooper-White J. Extensional properties of hydroxypropyl ether guar gum solutions. *Biomacromolecules*. 2008;9:2989-2996.

17. Vadillo DC, Tuladhar TR, Mulji AC, Jung S, Hoath SD, Mackley MR. Evaluation of the inkjet fluid's performance using the "Cambridge Trimaster" filament stretch and break-up device. *Journal of Rheology*. 2010;54(2):261.

18. Li J-M, Burghardt WR, Yang B, Khomami B. Flow birefringence and computational studies of a shear thinning polymer solution in axisymmetric stagnation flow. *Journal of Non-Newtonian Fluid Mechanics*. 1998;74(1):151-193.

19. Quinzani LM, McKinley GH, Brown RA, Armstrong RC. Modeling the rheology of polyisobutylene solutions. *Journal of Rheology*. 1990;34(5):705.

20. Holz T, Fischer P, Rehage H. Shear relaxation in the nonlinear-viscoelastic regime of a Giesekus fluid. *Journal of Non-Newtonian Fluid Mechanics*. 1999;88(1-2):133-148.

21. McKinley GH. Using filament stretching rheometry to predict strand formation and processability in adhesives and other non-Newtonian fluids. *Journal of Non-Newtonian Fluid Mechanics*. 2000;39:321-337.

22. Bird RB, Weist JM. Constitutive eqatuations for polymeric liquids. *Annual Review of Fluids Mechanics*. 1995;27:169-193.

23. Bird RB. Anisotropic Effects in Dumbbell Kinetic Theory. *Journal of Rheology*. 1985;29(5):519.

24. Wang Y, Xu J, Bechtel E, K.W. K. Melt shear rheology of carbon nanofiber/polyestyrene composites. *Rheologica Acta*. 2006;45:919-941.

25. Bird RB, Armstrong RC, Hassager O. *Dynamics of polymeric liquids. Volume 1 - Fluid Mechanics*. 2nd ed. John Wiley and Sons Inc.; 1987.

26. Nielsen LE. *Polymer Rheology*. New York: Marcel Dekker Inc.; 1977.

27. Entov VM, Hinch EJ. Effect of a spectrum of relaxation times on the capillary thinning of a filament of elastic liquid. *Journal of Non-Newtonian Fluid Mechanics*. 1997;72(1):31-53.

28. Warner HR. Kinetic Theory and Rheology of Dilute Suspensions of Finitely Extendible Dumbbells. *Industrial & Engineering Chemistry Fundamentals*. 1972;11(3):379-387.

29. Yao M, McKinley GH, Debbaut B. Extensional deformation, stress relaxation and necking failure of viscoelastic filaments. *Journal of Non-Newtonian Fluid Mechanics*. 1998;79(2-3):469-501.

30. Sachsenheimer D, Hochstein B, Buggisch H, Willenbacher N. Determination of axial forces during capillary breakup of liquid filaments – the tilted CaBER method. *Rheologica Acta*. 2012;51:909-923.

644 31. Clasen C, Eggers J, Fontelos MA, Li J, McKinley GH. The beads on a string structure of
645 viscoelastic threads. *Journal of Fluid Mechanics*. 2006;556:283-308.

646 32. Stelter M, Brenn G, Yarin AL, Singh RP, Durst F. Validation and application of a novel
647 elongational device for polymer solutions. *Journal of Rheology*. 2000;44:595.

648 33. McKinley GH, Tripathi A. How to extract the Newtonian viscosity from capillary breakup
649 measurements in a filament rheometer. *Journal of Rheology*. 2000;44(3):653.

650 34. Lindner A, Vermant J, Bonn D. How to obtain the elongational viscosity of dilute polymer
651 solutions? *Physica A*. 2003;319:125-133.

652 35. Szyszkowski B Von. Experimentelle Studien über kapillare Eigenschaften der wässrigen
653 Lösungen von Fettsäuren. *Z Phys Chem*. 1908;64:385-414.

654 36. Bouyer E, Mekhloufi G, Rosilio V, Grossiord J-L, Agnely F. Proteins, polysaccharides, and
655 their complexes used as stabilizers for emulsions: Alternatives to synthetic surfactants in the
656 pharmaceutical field? *International Journal of Pharmaceutics*. 2012;436(1):359-378.

657 37. Marangoni A, Narine S. *Physical properties of lipids*. Marcel Dekker Inc.; 2002.

658 38. Moreira R, Chenlo F, Silva C, et al. Surface tension and refractive index of guar and tragacanth
659 gums aqueous dispersions at different polymer concentrations, polymer ratios and
660 temperatures. *Food Hydrocolloids*. 2012;28(2):284-290.

661 39. Macosko CW. *Rheology: Principles, Measurements and Applications*. New York: Wiley VCH;
662 1994.

663 40. Ma X, Pawlik M. Intrinsic viscosities and Huggins constants of guar gum in alkali metal
664 chloride solutions. *Carbohydrate Polymers*. 2007;70(1):15-24.

665 41. Azevedo G, Bernardo G, Hilliou L. NaCl and KCl phase diagrams of kappa/iota-hybrid
666 carrageenans extracted from Mastocarpus stellatus. *Food Hydrocolloids*. 2014;37:116-123.

667 42. Dobrynin AV, Colby RH, Rubinstein M. Scaling theory of polyelectrolyte solutions.
668 *Macromolecules*. 1995;28:1859-1871.

669 43. Schleiniger G. A remark on the Giesekus viscoelastic fluid. *Journal of Rheology*.
670 1991;35(6):1157.

671 44. Yoo JY, Choi HC. On the steady simple shear flows of the one-mode Giesekus fluid.
672 *Rheologica Acta*. 1989;28(1):13-24.

673 45. Yesilata B, Clasen C, McKinley GH. Non linear shear and extensional flow dynamics of a
674 wormlike surfantact solutions. *Journal of Non-Newtonian Fluid Mechanics*. 2006;133:73-90.

675 46. Kheirandish S, Guybaidullin I, Willenbacher N. Shear and elongational flow behavior of
676 acrylic thickener solutions. Part II: effect of gel content. *Rheologica Acta*. 2009;48:397.

677 47. Haward SJ, Sharma V, Butts CP, McKinley GH, Rahatekar SS. Shear and Extensional
678 Rheology of Cellulose/Ionic Liquid Solutions. *Biomacromolecules*. 2012;13:1688-1699.

48. Trouton F. On the coefficient of viscous traction and its relation to that of viscosity. *Proceedings of the Royal Society of London Series A, Containing Papers of a Mathematical and Physical Character*. 1906;77(519):426-440.

Table captions

Table 1. Parameters obtained by fitting Equation (4) to guar gum and κ/ι-hybrid carrageenan solutions shear data in Figure 2.

Table 2. Values of power law factor, K^*, and power law exponent, n, required to estimate the relationship between material properties, $f(c)$, and solution concentration.

Table 3.Parameters obtained by fitting Equation (19) to guar gum solution extensional data in Figure 6 compared against those obtained using the shear data shown in Figure 2.

694 **Table 1.** Parameters obtained by fitting Equation (4) to guar gum and κ/ι-hybrid carrageenan solutions shear data in Figure 2.

Solution concentration C (g/L)	Mobility parameter a (-)	Relaxation time λ (s)	Surface tension α (N/m)	Zero shear rate viscosity η_0 (Pa s)	Initial filament diameter D_1 (μm)	R^2 value (-)
Guar gum						
1	0.00035±0.00001[d]	0.090±0.003[f]	0.0685±0.0002[a]	0.0029±0.0002[f]	205±2[f]	0.993
2	0.0026±0.0002[c]	0.150±0.002[e]	0.0675±0.0003[b]	0.022±0.003[e]	280±3[e]	0.992
5	0.051±0.002[b]	0.878±0.002[d]	0.0675±0.0002[b]	0.480±0.004[d]	430±1[d]	0.988
10	0.50±0.00[a]	2.37±0.01[c]	0.0674±0.0001[b]	5.87±0.05[c]	477±3[c]	0.950
15	0.50±0.00[a]	14.5±0.1[b]	0.0673±0.0001[b]	89.5±0.2[b]	482±1[b]	0.891
20	0.50±0.00[a]	18.2±0.2[a]	0.0672±0.0001[b]	550±12[a]	487±2[a]	0.886
κ/ι-hybrid carrageenan gum						
5	0.0029±0.0004[d]	0.312±0.003[d]	0.0725±±0.0002[a]	0.040±0.002[d]	316±1[b]	0.995
10	0.021±0.002[c]	2.33±0.05[c]	0.0714±±0.0002[b]	0.381±0.003[c]	319±1[a,b]	0.996
15	0.18±0.01[b]	8.24±0.04[b]	0.0709±±0.0002[c]	3.85±0.04[b]	321±1[a]	0.993
20	0.495±0.00[a]	13.55±0.06[a]	0.0703±±0.0002[d]	14.1±0.1[a]	324±2[a]	0.990

695 [†]Data are presented as mean ± standard deviation. Data values in a column with different superscript letters are significantly different at the $p \leq 0.05$ level.

696

Table 2. Values of power law factor, K^*, and power law exponent, n, required to estimate the relationship between material properties, $f(c)$, and solution concentration.

	guar gum		κ/ι-hybrid carrageenan gum	
Parameter	K^*	n	K^*	n
Zero shear rate viscosity, η_0	$(2.60 \pm 0.02) \times 10^{-3}$	3.30±0.03	$(4.01 \pm 0.03) \times 10^{-5}$	3.75±0.02
Mobility parameter, a	$(3.20 \pm 0.01) \times 10^{-4}$	3.17±0.05	$(9.05 \pm 0.02) \times 10^{-6}$	3.60±0.03
Relaxation time, λ	$(7.37 \pm 0.04) \times 10^{-2}$	1.49±0.10	$(3.7 \pm 0.03) \times 10^{-3}$	2.79±0.08

Units of K^* are [parameter] $(g/L)^{-n}$

703 **Table 3.** Parameters obtained by fitting Equation (19) to guar gum solution extensional data in Figure 6 compared against those obtained using the shear data
704 shown in Figure 2.

Concentration	Shear flow (Figure 2)		Extensional shear (Figure 6)		R^2 value
C	a	λ	a	λ	
(g/L)	(-)	(s)	(-)	(s)	(-)
5	0.051±0.002[b]	0.878±0.002[b]	0.032±0.005[b]	0.029±0.001[a]	0.994
10	0.50±0.00[a]	2.37±0.01[a]	0.461±0.003[a]	0.023±0.002[a]	0.995

705 †Data are presented as mean ± standard deviation. Data values in a column with different superscript letters are significantly different at the $p \leq 0.05$ level.
706

Figure captions

Figure 1 Effect of guar gum (circles) and κ/ι-hybrid carrageenan gum (triangles) concentration on reduced viscosity. Data points for guar gum are computed from experimental η_0 data from Torres and co-workers[1]. Dashed lines are fits of Equation (23) to the first three data points for guar gum solutions and to the whole set of data for κ/ι-hybrid carrageenan gum solutions.

Figure 2 Comparison of the measured apparent viscosity of (*a*) guar gum solutions (reproduced from Torres and co-workers[1]) and (*b*) κ/ι-hybrid carrageenan gum solutions with the Giesekus model, Equation(4). Concentration: 1 g/L (open grey circles); 2 g/L (open black triangles); 5 g/L (open grey squares); 10 g/L (open black diamonds); 15 g/L (dashes) and 20 g/L (crosses). Dashed loci indicate model fit, parameters in Table 1.

Figure 3 Effect of concentration on Giesekus model parameters. (*a*) η_0; (*b*) a and (*c*) λ for guar gum and κ/ι-hybrid carrageenan gum. Dashed loci shows the power law trend line, Equation (24), fitted to the data for solutions in the semi-dilute regime, parameters given in Table 1. Symbols: circles – guar gum solutions, triangles - κ/ι-hybrid carrageenan gum solutions.

Figure 4 Normal stress differences (N_1-N_2) measured for aqueous (a) κ/ι-hybrid carrageenan gum and (b) guar gum solutions prepared at different polymer concentration. Lines show the difference between Equations (7) and (8) fitted to the data for studied solutions. Concentration: 2 g/L (open black triangles); 5 g/L (open grey squares); 10 g/L (open black diamonds); 15 g/L (dashes) and 20 g/L (crosses). The dashed horizontal line corresponds to the noise floor of the normal force transducer.

Figure 5 Comparison of measured non-dimensional filament diameter with Giesekus model, Equation (19) for (*a*) κ/ι-hybrid carrageenan gum solutions, (*b*) guar gum solutions, semi-dilute regime; (*c*) guar gum solutions, entangled regime. Concentration: 1 g/L (open grey circles); 2 g/L (open black triangles); 5 g/L (open grey squares); 10 g/L (open black diamonds); 15 g/L (dashes) and 20 g/L (crosses). Dashed loci show predictions from Equation (19) using the parameters obtained from steady shear studies given in Table 1.

739 **Figure 6** Fitting of guar gum solution filament stretching data in Figure 4(*c*) to Equation (19) when
740 Giesekus model parameters a and λ are allowed to differ from those obtained from fitting
741 shear flow data (Figure (2*a*)). Dashed loci – model fit with parameters given in Table 3.
742
743 **Figure 7** Time-concentration superposition of the filament stretching data in Figure 5, where time is
744 normalised by the experimental filament rupture time: (*a*) κ/ι-hybrid carrageenan gum and
745 (*b*) guar gum (reproduced from Torres and co-workers[1]).
746
747 **Figure 8** Relationship between filament rupture time, obtained from extensional testing, and mobility
748 parameter obtained from shear flow data. Symbols: circles – guar gum, triangles - κ/ι-hybrid
749 carrageenan gum solutions
750
751 **Figure 9** Comparison of the left- and right-hand sides of Equation (25) for (*a*) κ/ι-hybrid carrageenan
752 gum and (*b*) guar gum solutions. Open circles – guar gum in semi-dilute region; solid
753 circles – guar gum in entangled regime; triangles – κ/ι-hybrid carrageenan. Labels indicate
754 gum concentration.
755
756 **Figure 10** Effect of Hencky strain on Trouton ratio, for different guar gum concentrations. Symbols
757 show experimental data reported by Torres and co-workers[1]. Solid loci represent predictions
758 of the Trouton ratio *via* Equation (4) and Equation (22)
759
760

761 *(a)*

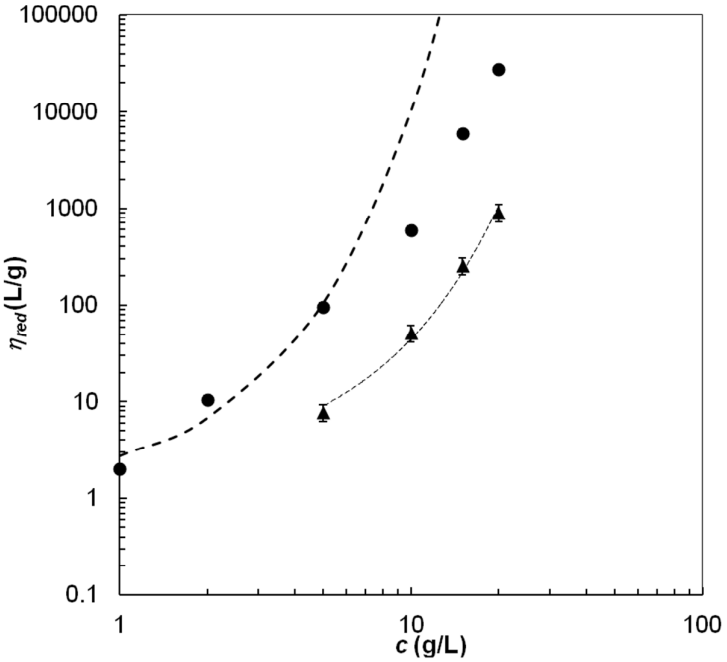

762

763 *(b)*

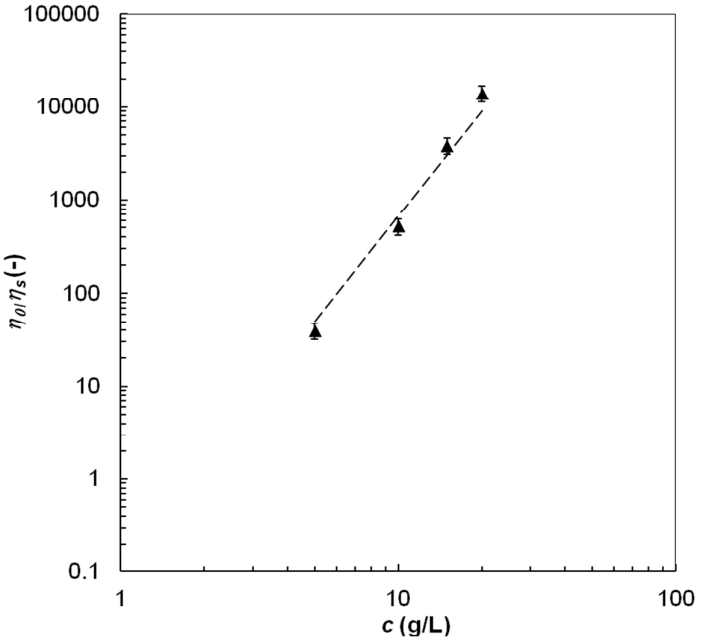

764

765 **Figure 1** Effect of guar gum (circles) and κ/ι-hybrid carrageenan gum (triangles) concentration on
766 reduced viscosity. Data points for guar gum are computed from experimental η_0 data from
767 Torres and co-workers[1]. Dashed lines are fits of Equation (23)to the first three data points
768 for guar gum solutions and to the whole set of data for κ/ι-hybrid carrageenan gum
769 solutions.

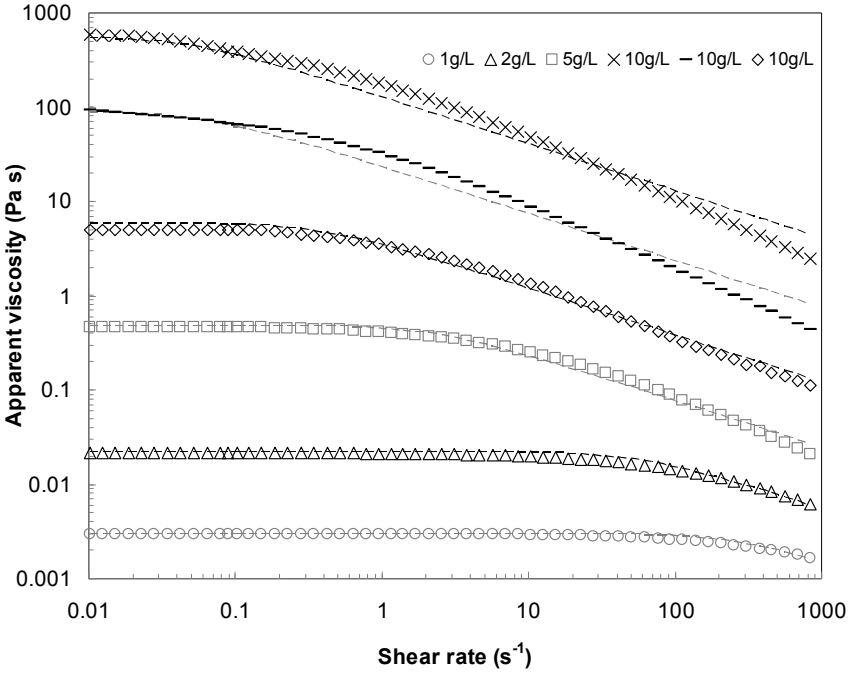

(*b*)

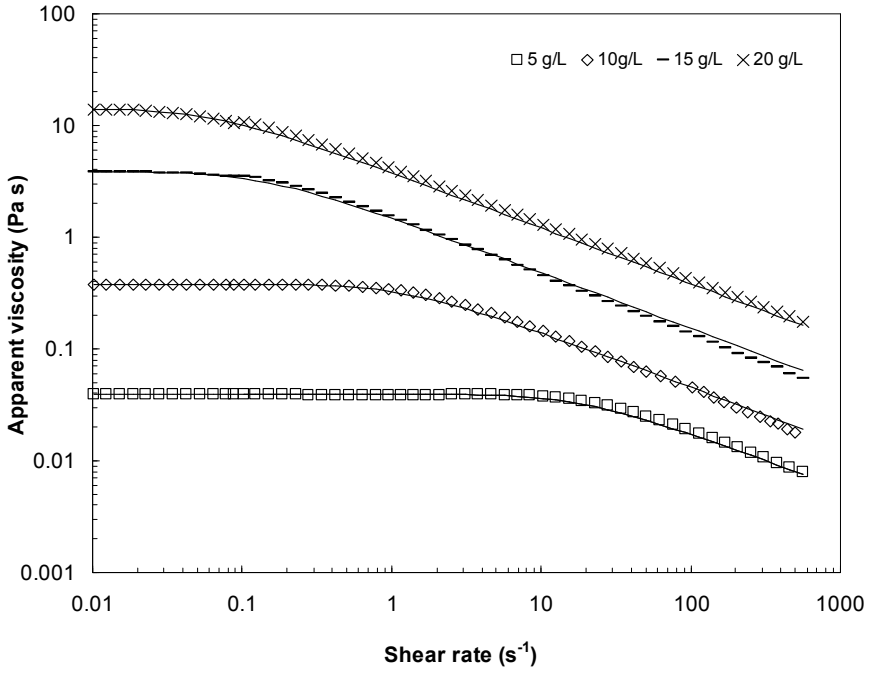

Figure 2 Comparison of the measured apparent viscosity of (*a*) guar gum solutions (reproduced from Torres and co-workers[1]) and (*b*) κ/ι-hybrid carrageenan gum solutions with the Giesekus model, Equation(4). Concentration: 1g/L (open grey circles); 2g/L (open black triangles); 5g/L (open grey squares); 10g/L (open black diamonds); 15 g/L (dashes) and 20 g/L (crosses). Dashed loci indicate model fit, parameters in Table 1.

779 (*a*)

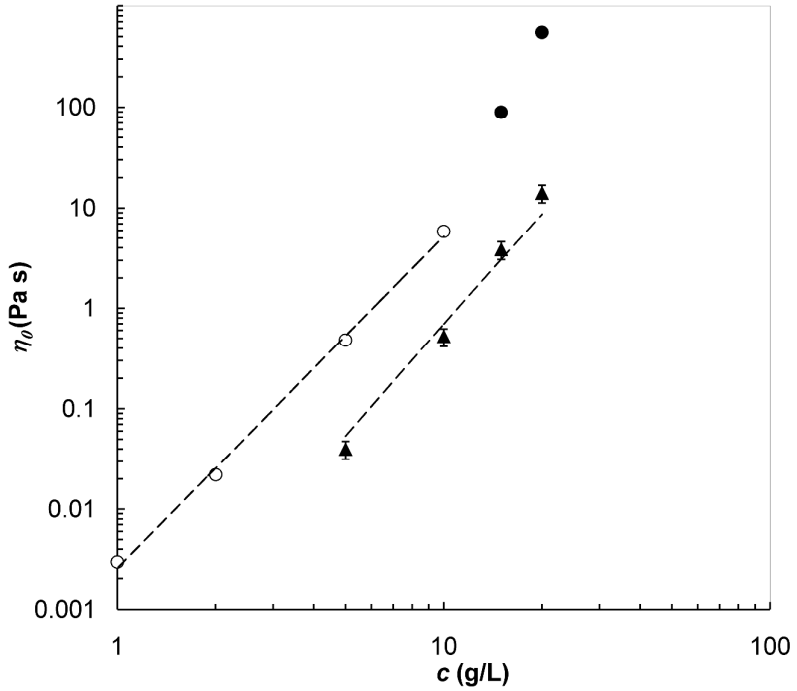

780

781 (*b*)

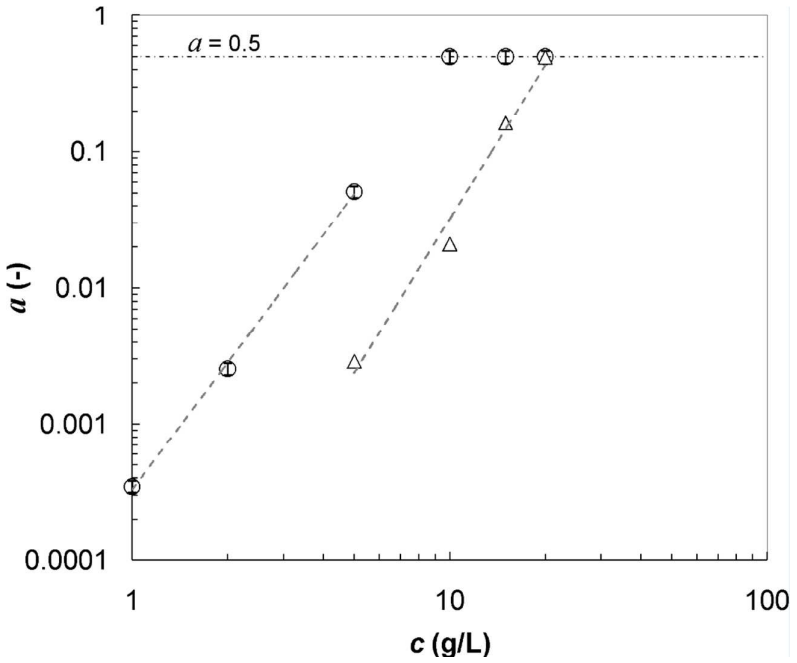

782

783

784 (*c*)

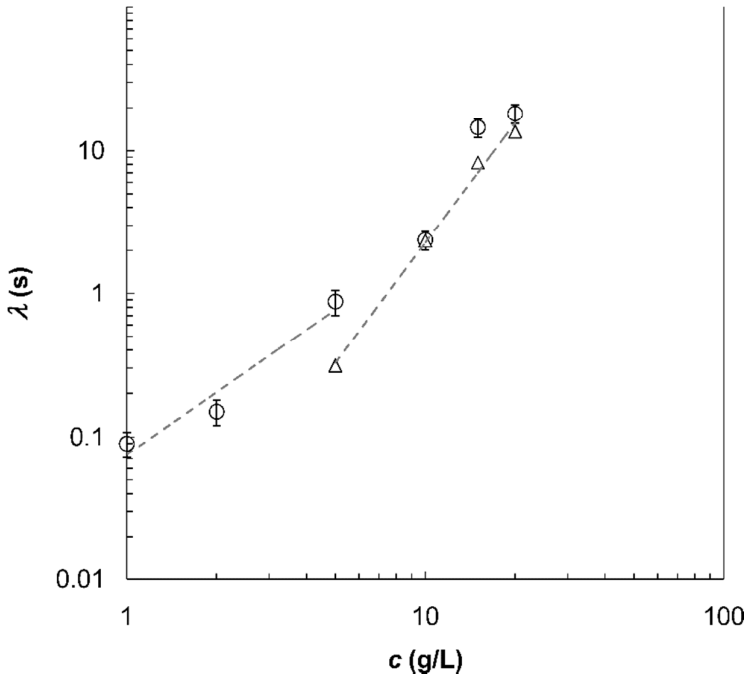

785

786 **Figure 3** Effect of concentration on Giesekus model parameters. (*a*) η_0; (*b*) *a* and (*c*) $\lambda$for guar gum
787 and κ/ι-hybrid carrageenan gum. Dashed loci shows the power law trend line, Equation (24),
788 fitted to the data for solutions in the semi-dilute regime, parameters given in Table 1.
789 Symbols: circles – guar gum solutions, triangles - κ/ι-hybrid carrageenan gum solutions.

790

791

792 *(a)*

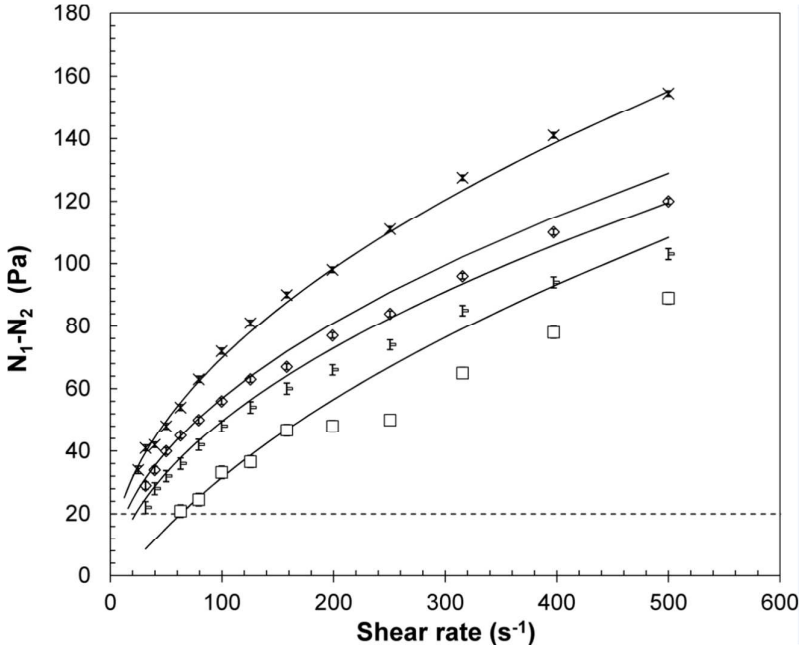

793

794 *(b)*

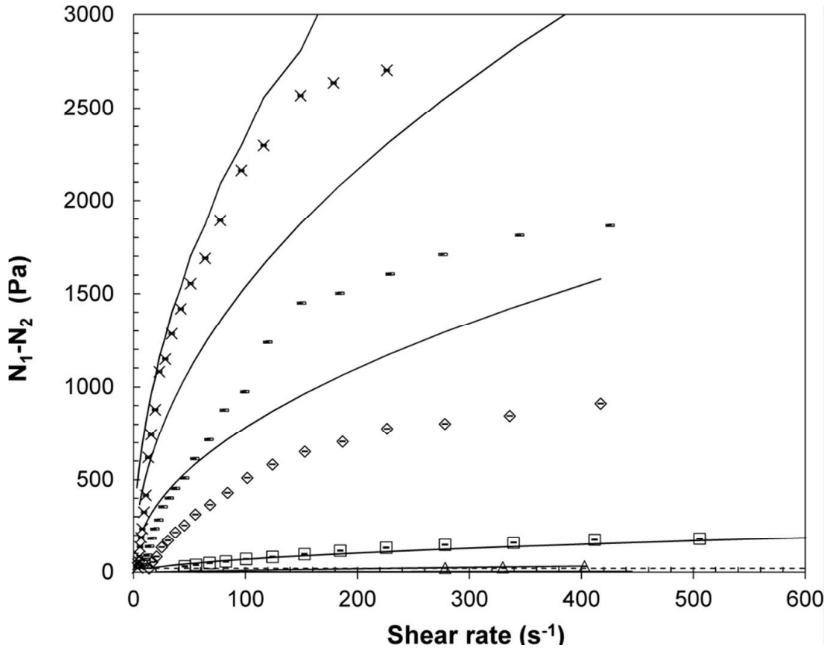

795

796 **Figure 4** Normal stress differences (N_1-N_2) measured for aqueous (*a*) κ/ι-hybrid carrageenan gum and
797 (*b*) guar gum solutions prepared at different polymer concentration. Lines show the difference
798 between Equations (7) and (8) fitted to the data for studied solutions. Concentration: 2 g/L
799 (open black triangles); 5 g/L (open grey squares); 10 g/L (open black diamonds); 15 g/L
800 (dashes) and 20 g/L (crosses). The dashed horizontal line corresponds to the noise floor of
801 the normal force transducer.

802

803 *(a)*

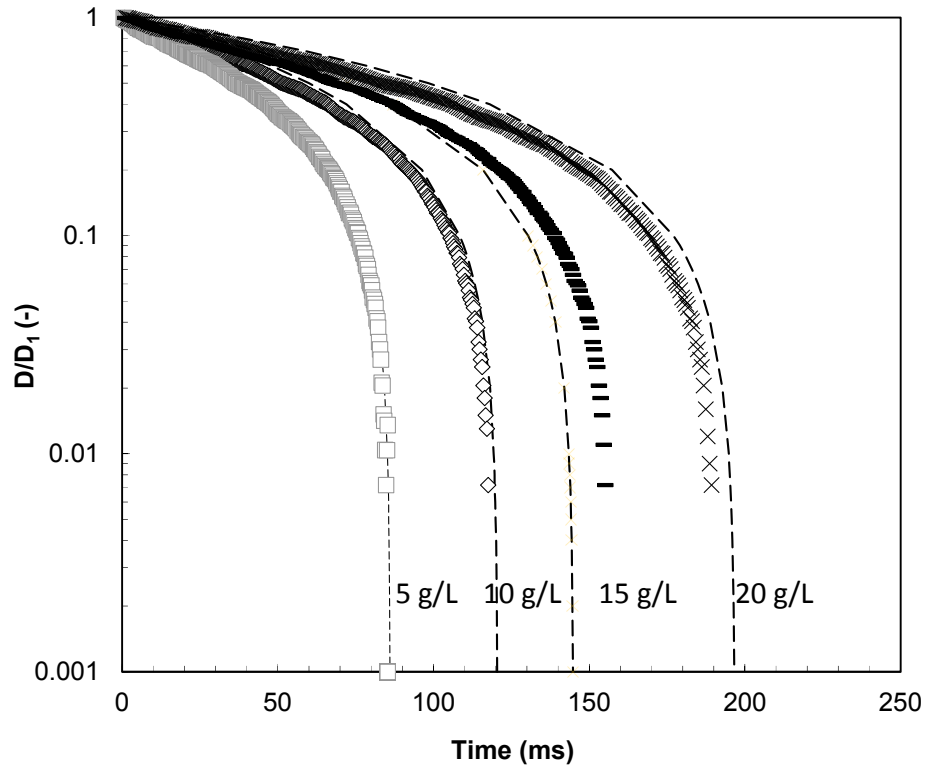

804

805 (*b*)

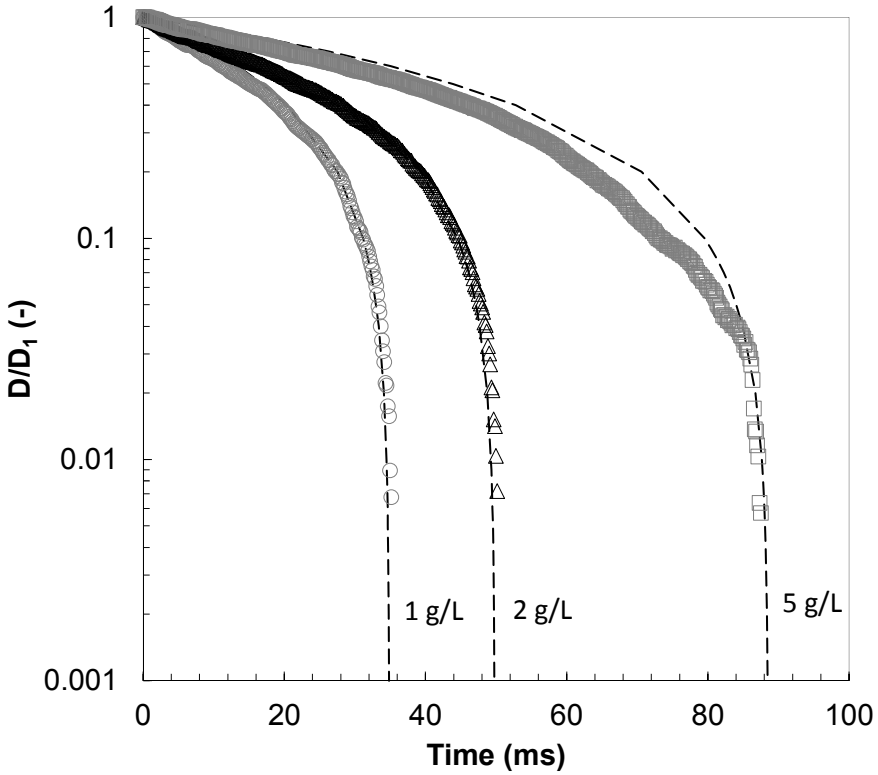

806

807 (*c*)

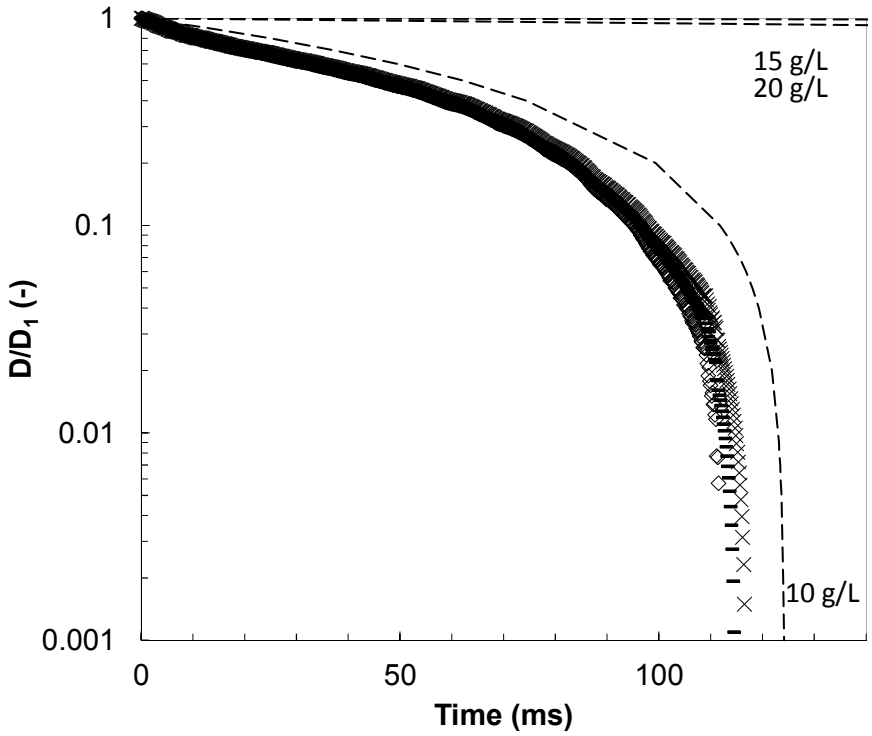

808
809

810 **Figure 5** Comparison of measured non-dimensional filament diameter with Giesekus model,
811 Equation (19) for (*a*) κ/ι-hybrid carrageenan gum solutions, (*b*) guar gum solutions, semi-
812 dilute regime; (*c*) guar gum solutions, entangled regime. Concentration: 1 g/L (open grey
813 circles); 2 g/L (open black triangles); 5 g/L (open grey squares); 10 g/L (open black
814 diamonds); 15 g/L (dashes) and 20 g/L (crosses). Dashed loci show predictions from
815 Equation (19) using the parameters obtained from steady shear studies given in Table 1.
816

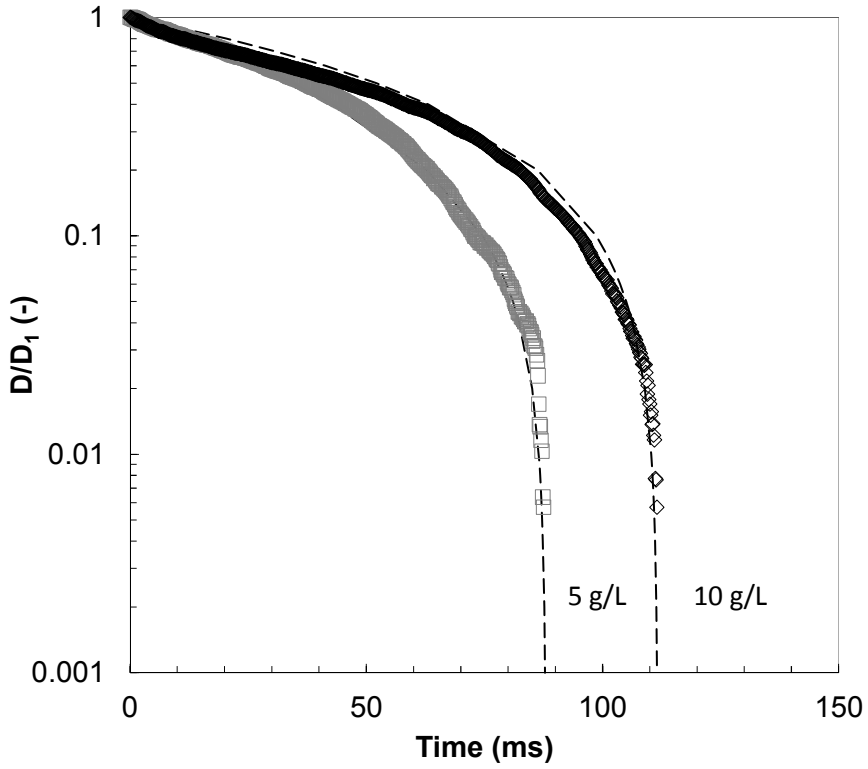

817

818 **Figure 6** Fitting of guar gum solution filament stretching data in Figure 4(*c*) to Equation (19) when
819 Giesekus model parameters a and λ are allowed to differ from those obtained from fitting
820 shear flow data (Figure 2(*a*)). Dashed loci – model fit with parameters given in Table 3.
821

822 (*a*)

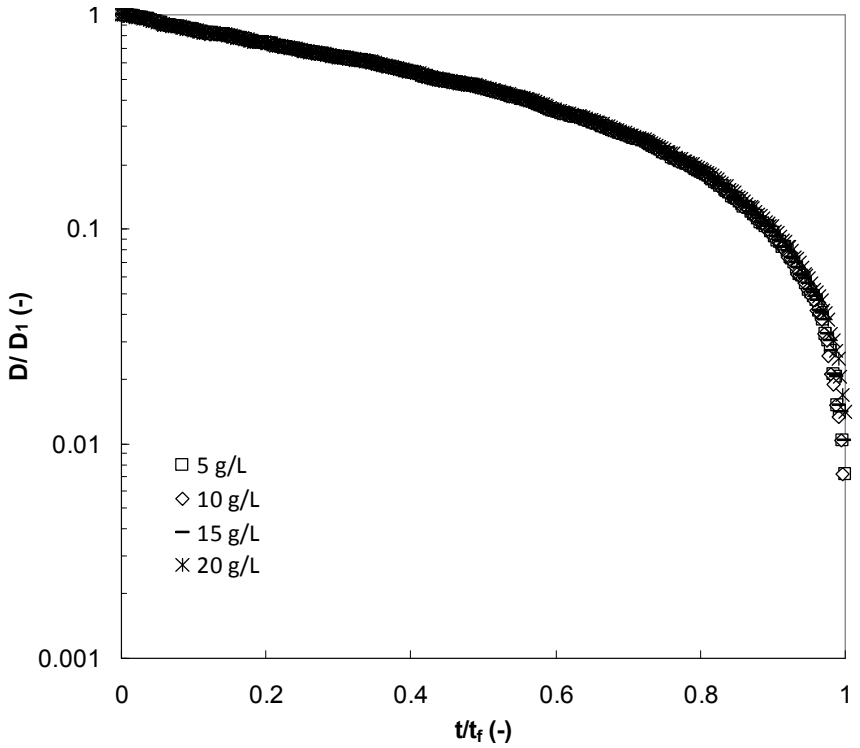

823

824 (*b*)

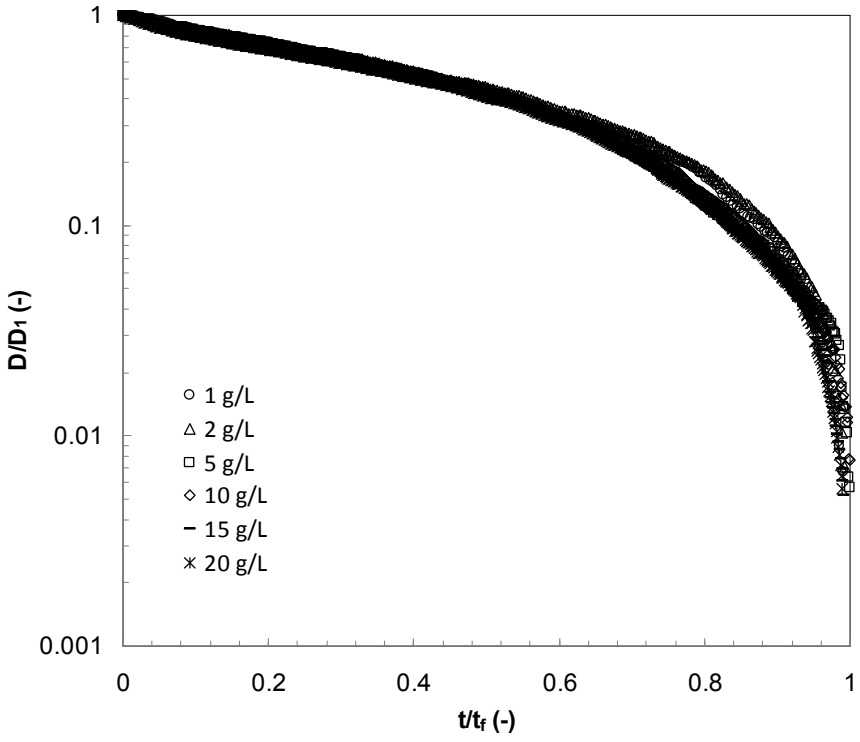

825

826 **Figure 7** Time-concentration superposition of the filament stretching data in Figure 5, where time is
827 normalised by the experimental filament rupture time: (*a*) κ/ι-hybrid carrageenan gum and
828 (*b*) guar gum (reproduced from Torres and co-workers[1]).

829

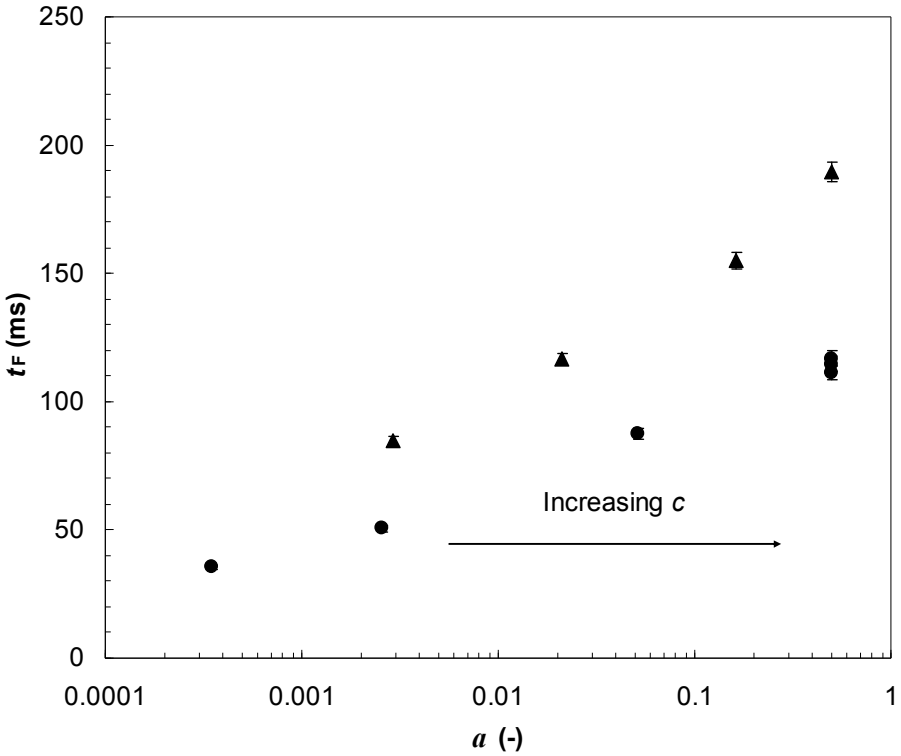

Figure 8 Relationship between filament rupture time, obtained from extensional testing, and mobility parameter obtained from shear flow data. Symbols: circles – guar gum, triangles - κ/ι-hybrid carrageenan gum solutions.

835 *(a)*

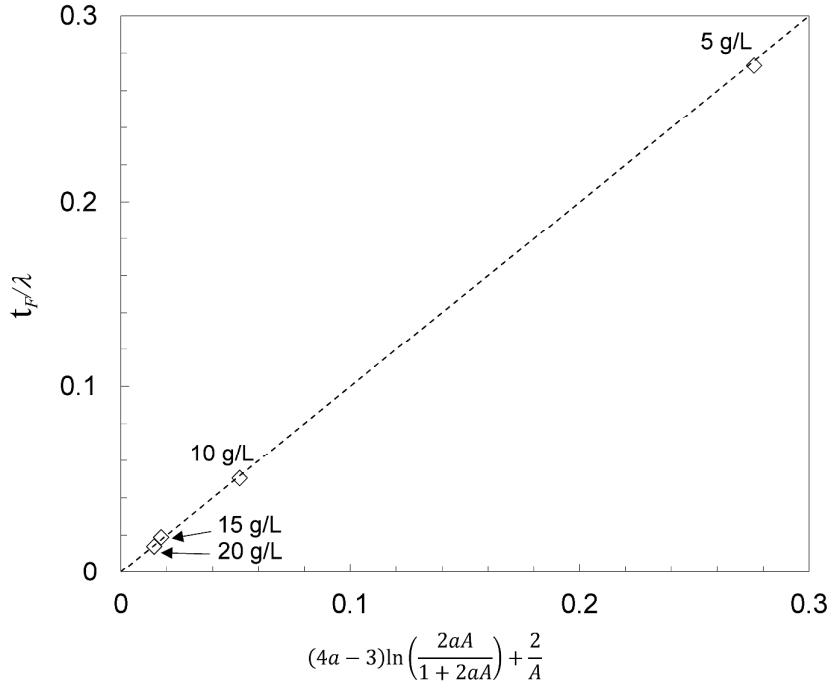

836

837 *(b)*

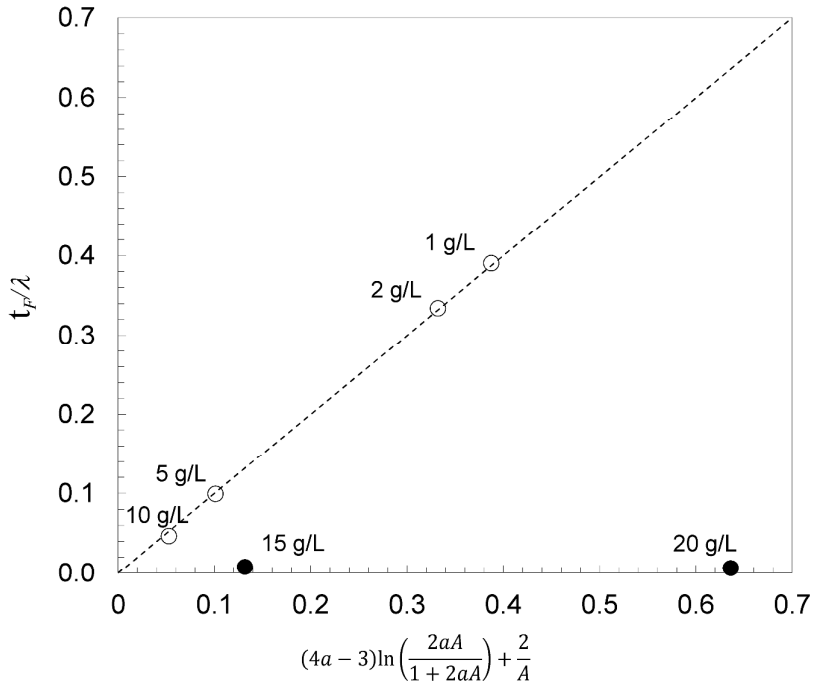

838

839 **Figure 9** Comparison of the left- and right-hand sides of Equation (25) for (*a*) κ/ι-hybrid carrageenan
840 gum and (*b*) guar gum solutions. Open circles – guar gum in semi-dilute region; solid
841 circles – guar gum in entangled regime; diamonds – κ/ι-hybrid carrageenan. Labels indicate
842 gum concentration.

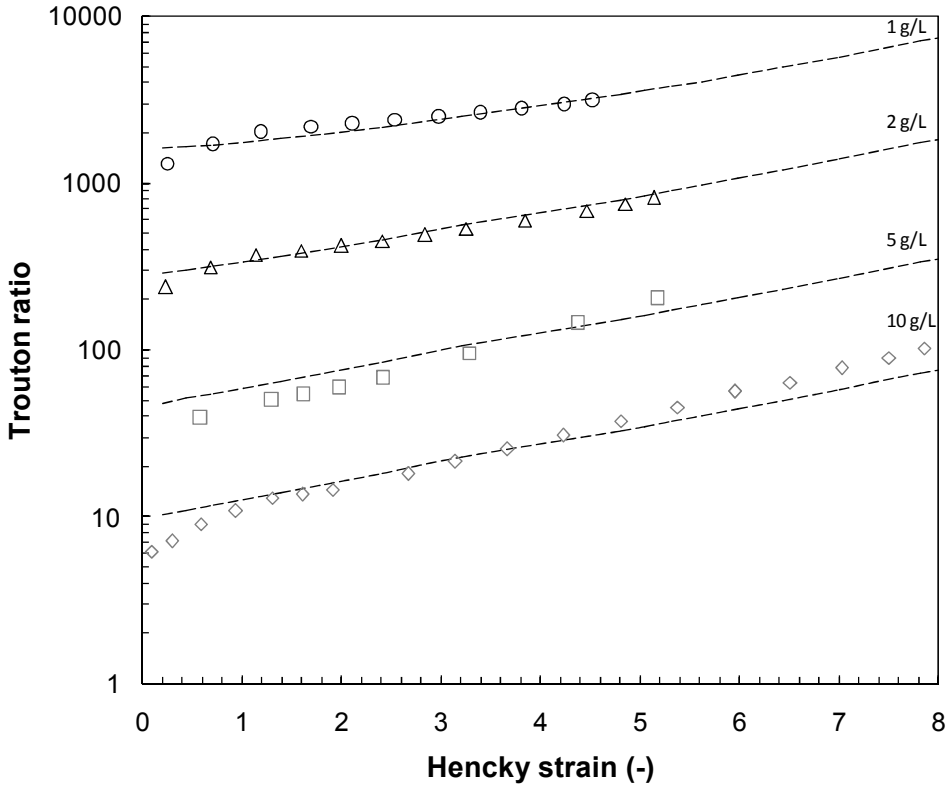

843

844 **Figure 10** Effect of Hencky strain on Trouton ratio, for different guar gum concentrations. Symbols
845 show experimental data reported by Torres and co-workers[1]. Solid loci represent predictions
846 of the Trouton ratio *via* Equation (4) and Equation (22)

847

Appendix

Surface tension

The surface tension between the κ/ι-hybrid carrageenan gum solutions and air at 21°C was determined experimentally using the sessile drop method with a Kruss Drop Shape Analyser 100 device. Values reported are the mean from at least ten measurements. The influence of κ/ι-hybrid carrageenan gum concentration was satisfactorily fitted to the Szyszkowski equation[35]:

$$\frac{\alpha}{\alpha_0} = 1 - s_1 \ln\left(1 + \frac{c}{s_2}\right) \qquad \text{(A.1)}$$

where α_0 is the surface tension of the solvent, c the concentration of the surfactant and $s_1$and s_2 are fitting parameters.

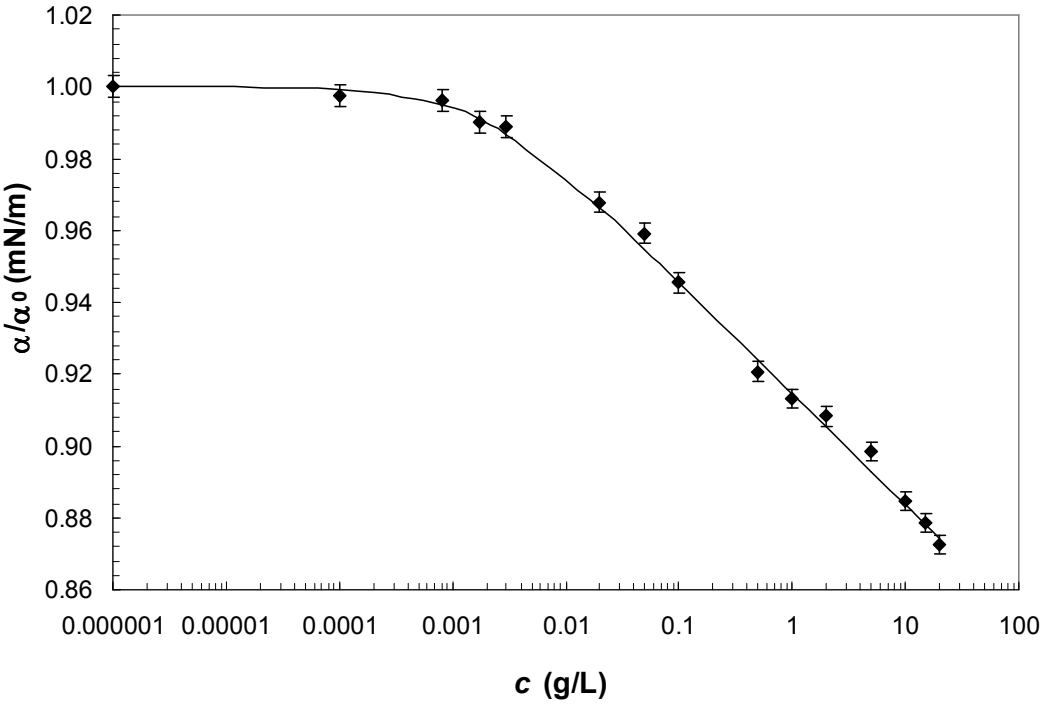

Figure A.1. Effect of κ/ι-hybrid carrageenan gum concentration on surface tension relative to water. Solid trend line shows Equation (A.1) fitted to the κ/ι-hybrid carrageenan gum data with parameters s_1 = 0.0135 and s_2= 0.0018 g/L.

Cross model

The experimental flow curves for κ/ι-hybrid carrageenan gum samples were satisfactorily fitted (R^2> 0.990, standard error < 0.0023 Pa s) to the Cross-Williamson model, Eqn. (A.2),

$$\frac{\eta_{app}}{\eta_0} = \frac{1}{1 + k_c \dot{\gamma}^{(1-n)}} \qquad \text{(A.2)}$$

where $\eta_0$is the zero-shear rate viscosity, k_c is the time constant and n is the flow index.

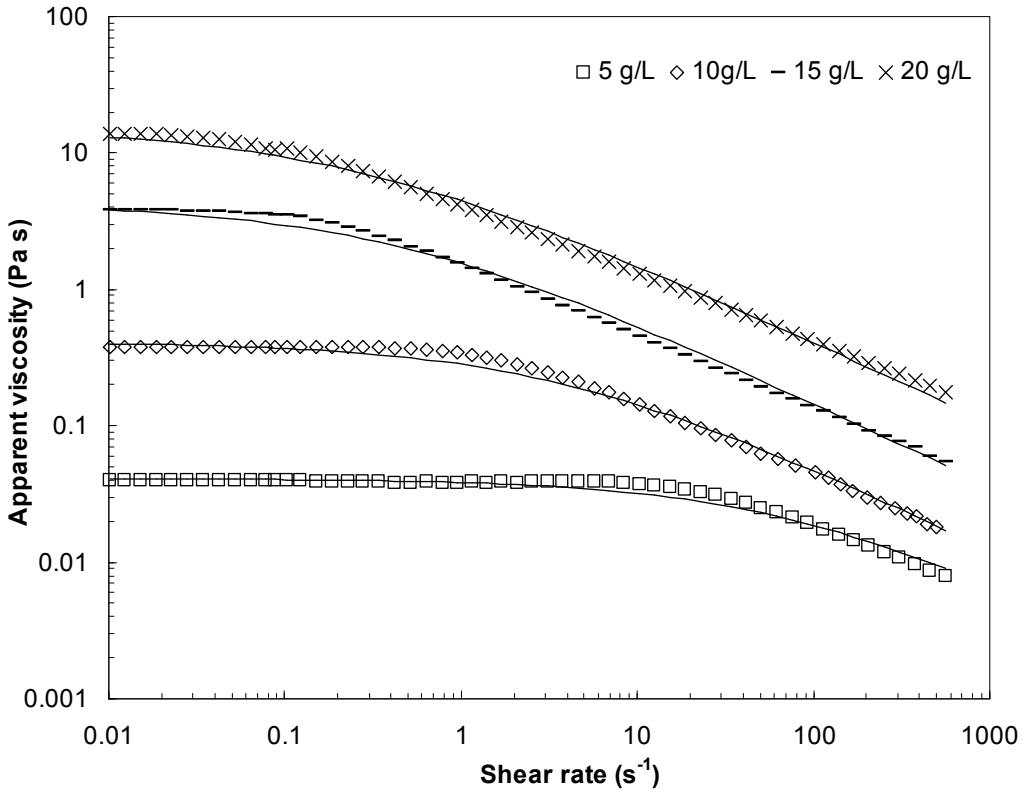

Figure A.2. Flow curves of representative aqueous κ/ι-hybrid carrageenan gum solutions prepared at different concentrations. Symbols: 5 g/L (squares); 10 g/L (diamonds); 15 g/L (dashes) and 20 g/L (crosses). Dashed loci indicate model fit obtained using Cross model, Equation (A.2), parameters in Table A.1.

874

875 **Table A.1** Parameter values obtained for Cross-Williamson model, Equation (A.2), for aqueous κ/ι-
876 hybrid carrageenan gum solutions prepared at different concentration. †

c (g/L)	η_0 (Pa s)	k_c (s^{1-n})	n (-)	R^2	s (Pa s)
5	0.041±0.02^{d}	0.066±0.002^{d}	0.37±0.01^{b}	0.996	0.0015
10	0.41±0.03^{c}	0.45±0.02^{c}	0.38±0.01^{a,b}	0.995	0.0018
15	4.2±0.2^{b}	1.7±0.1^{b}	0.39±0.01^{a}	0.990	0.0023
20	15.1±0.3^{a}	2.4±0.1^{a}	0.41±0.01^{a,b}	0.991	0.0021

877 †Data are presented as mean ± standard deviation. Data values in a column
878 with different superscript letters are significantly different at the $p \leq 0.05$
879 level.
880

881 ***Trouton ratio***

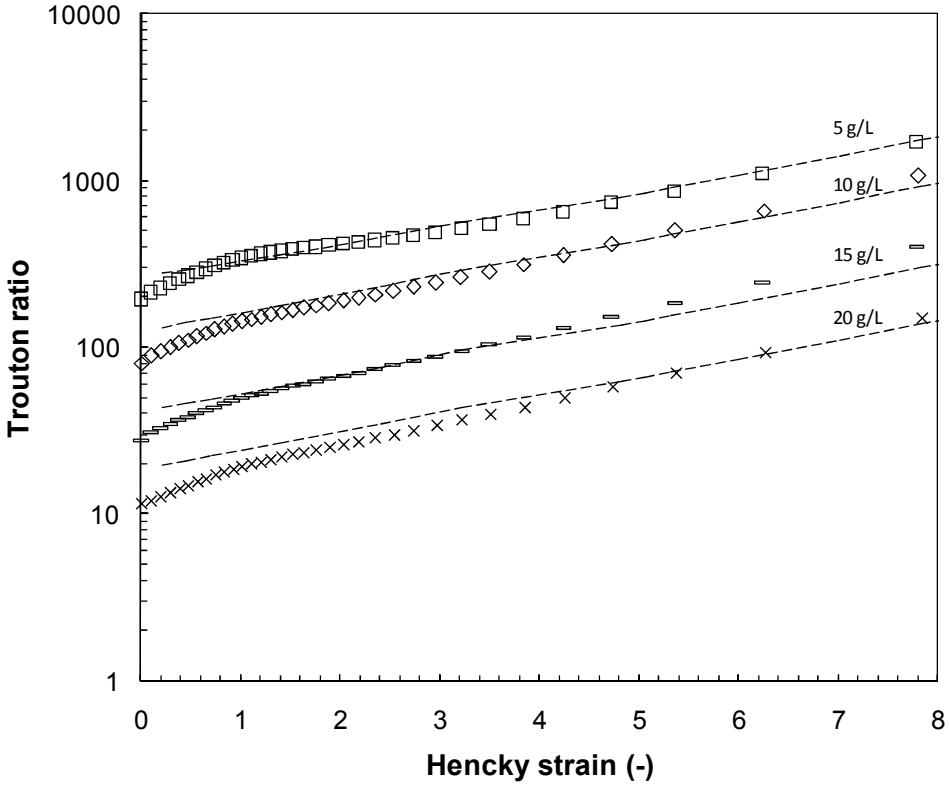

882

883 **Figure A.3.** Effect of Hencky strain on Trouton ratio, for different κ/ι-hybrid carrageenan gum
884 concentrations. Symbols: 5 g/L (squares); 10 g/L (diamonds); 15 g/L (dashes) and 20 g/L
885 (crosses). Solid loci represent predictions of the Trouton ratio *via* Equation (4) and Equation
886 (21)

887

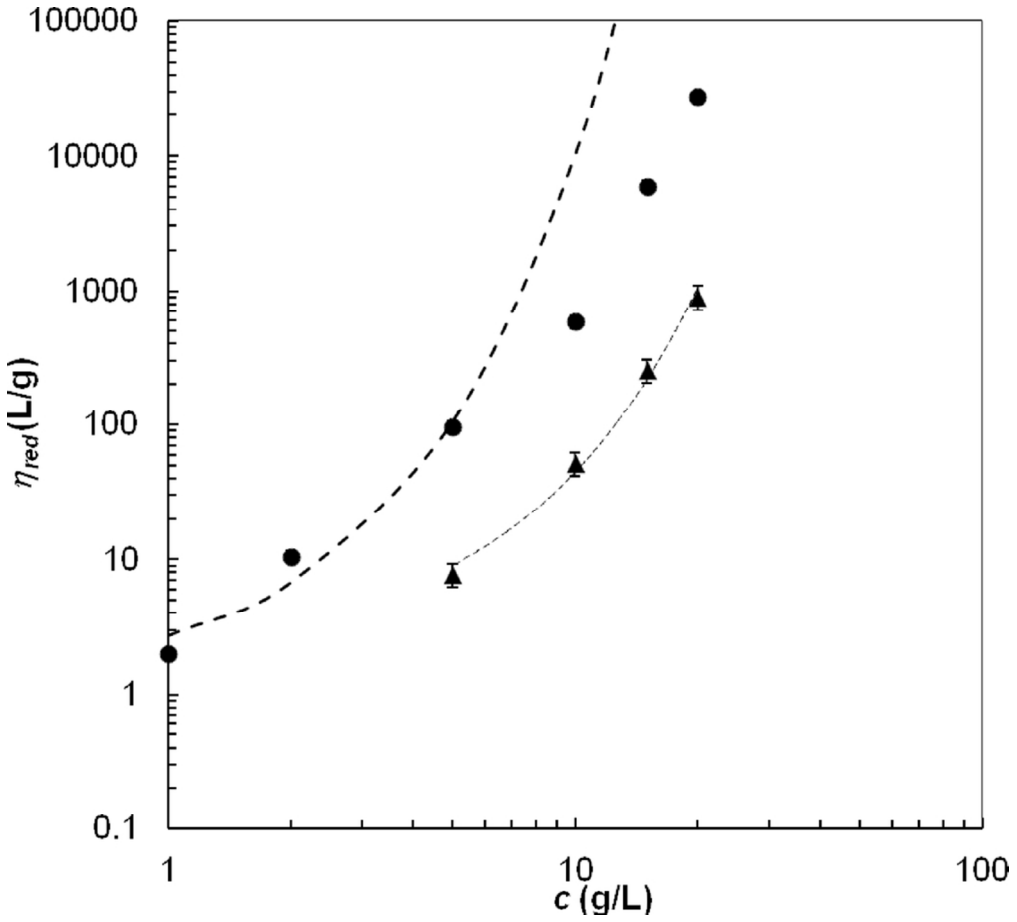

Figure 1a. Effect of guar gum (circles) and κ/ι-hybrid carrageenan gum (triangles) concentration on reduced viscosity. Data points for guar gum are computed from experimental η_0 data from Torres and co-workers[1]. Dashed lines are fits of Equation (23) to the first three data points for guar gum solutions and to the whole set of data for κ/ι-hybrid carrageenan gum solutions.
87x79mm (300 x 300 DPI)

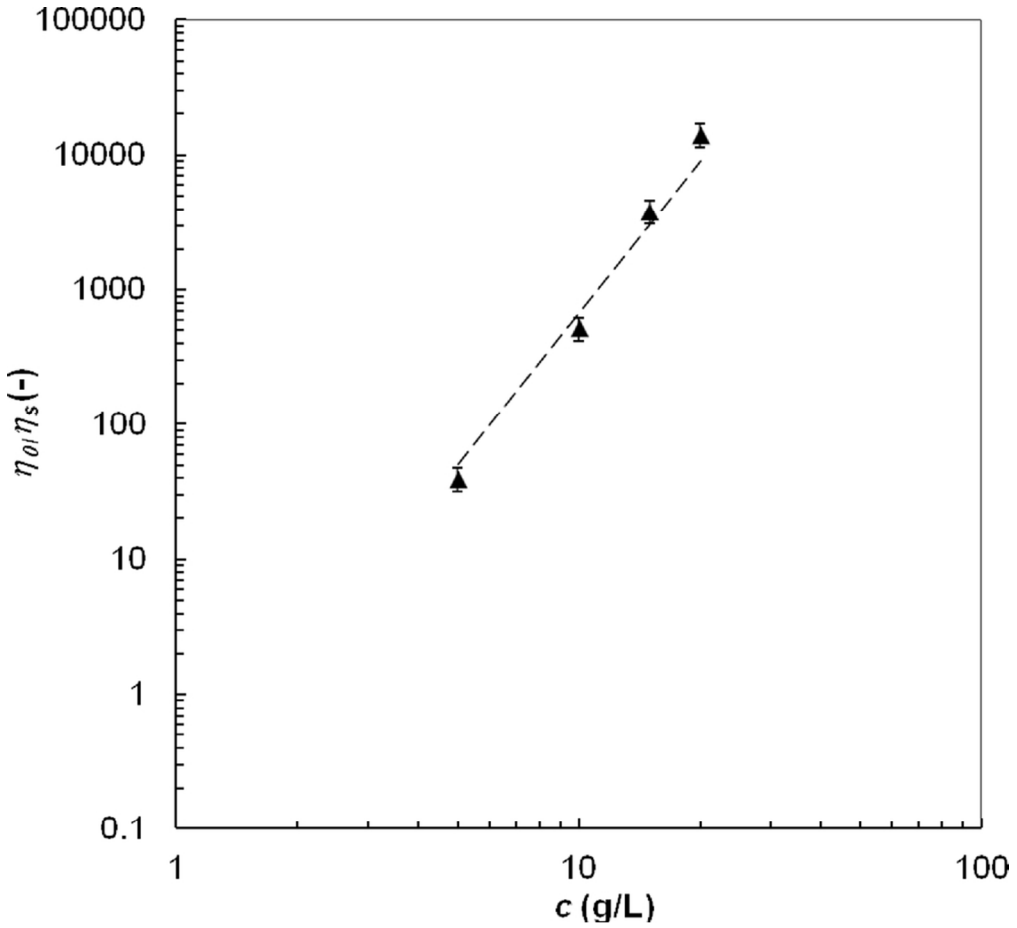

Figure 1b. Effect of guar gum (circles) and κ/ι-hybrid carrageenan gum (triangles) concentration on reduced viscosity. Data points for guar gum are computed from experimental η_0 data from Torres and co-workers[1]. Dashed lines are fits of Equation (23) to the first three data points for guar gum solutions and to the whole set of data for κ/ι-hybrid carrageenan gum solutions.
83x76mm (300 x 300 DPI)

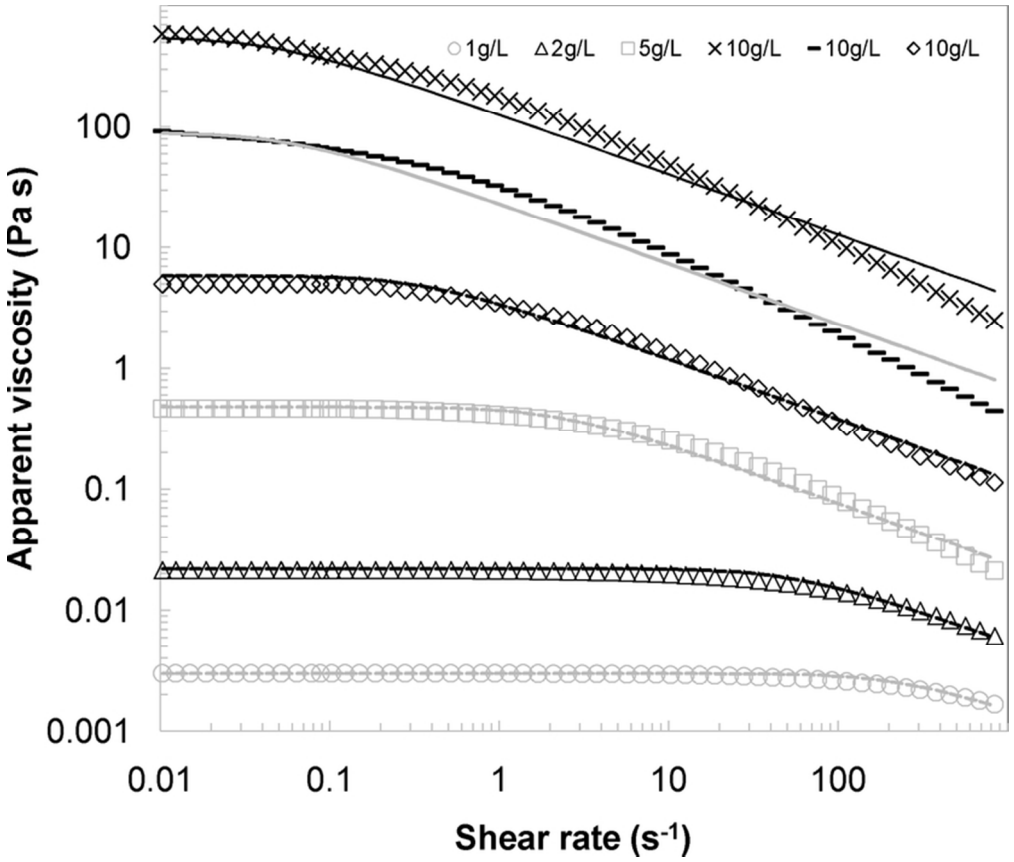

Figure 2a. Comparison of the measured apparent viscosity of guar gum solutions (reproduced from Torres and co-workers[1]) with the Giesekus model, Equation (4). Concentration: 1 g/L (open grey circles); 2 g/L (open black triangles); 5 g/L (open grey squares); 10 g/L (open black diamonds); 15 g/L (dashes) and 20 g/L (crosses). Dashed loci indicate model fit, parameters in Table 1.
70x59mm (300 x 300 DPI)

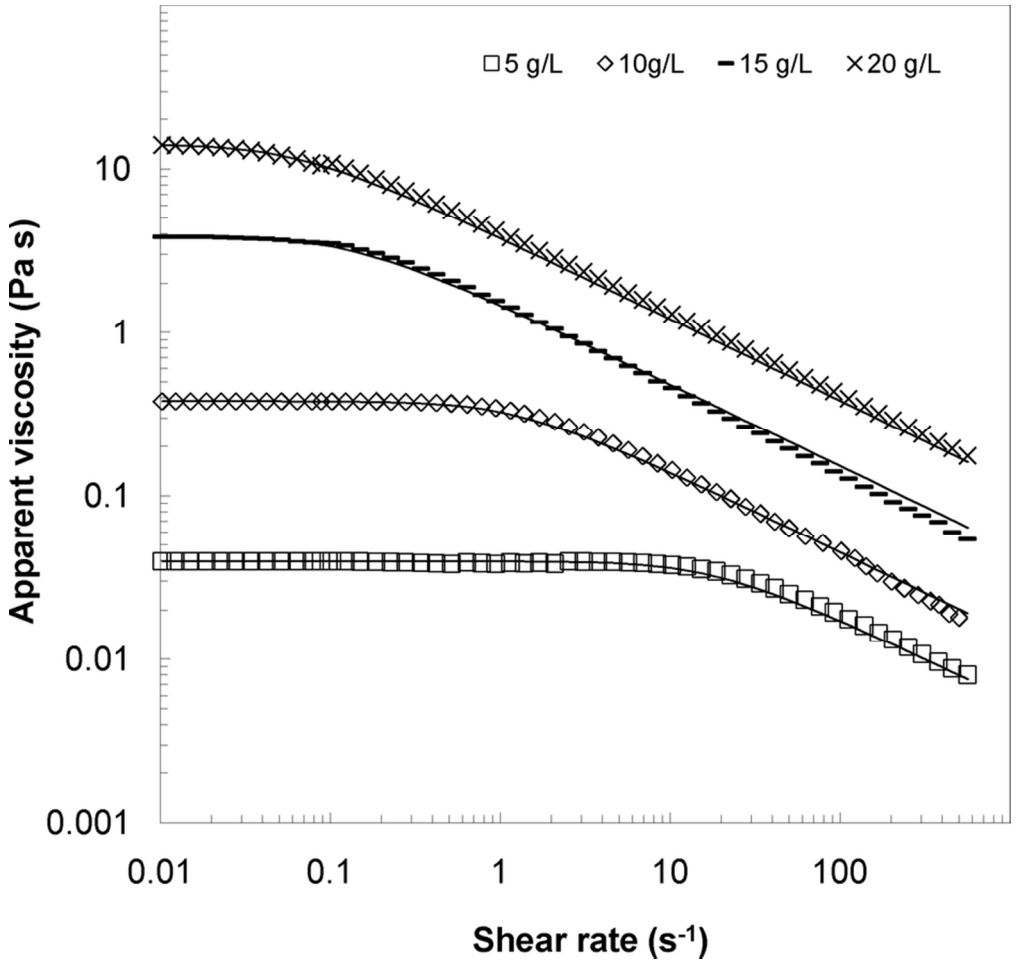

Figure 2b. Comparison of the measured apparent viscosity of κ/ι-hybrid carrageenan gum solutions with the Giesekus model, Equation (4). Concentration: 1 g/L (open grey circles); 2 g/L (open black triangles); 5 g/L (open grey squares); 10 g/L (open black diamonds); 15 g/L (dashes) and 20 g/L (crosses). Dashed loci indicate model fit, parameters in Table 1.
79x75mm (300 x 300 DPI)

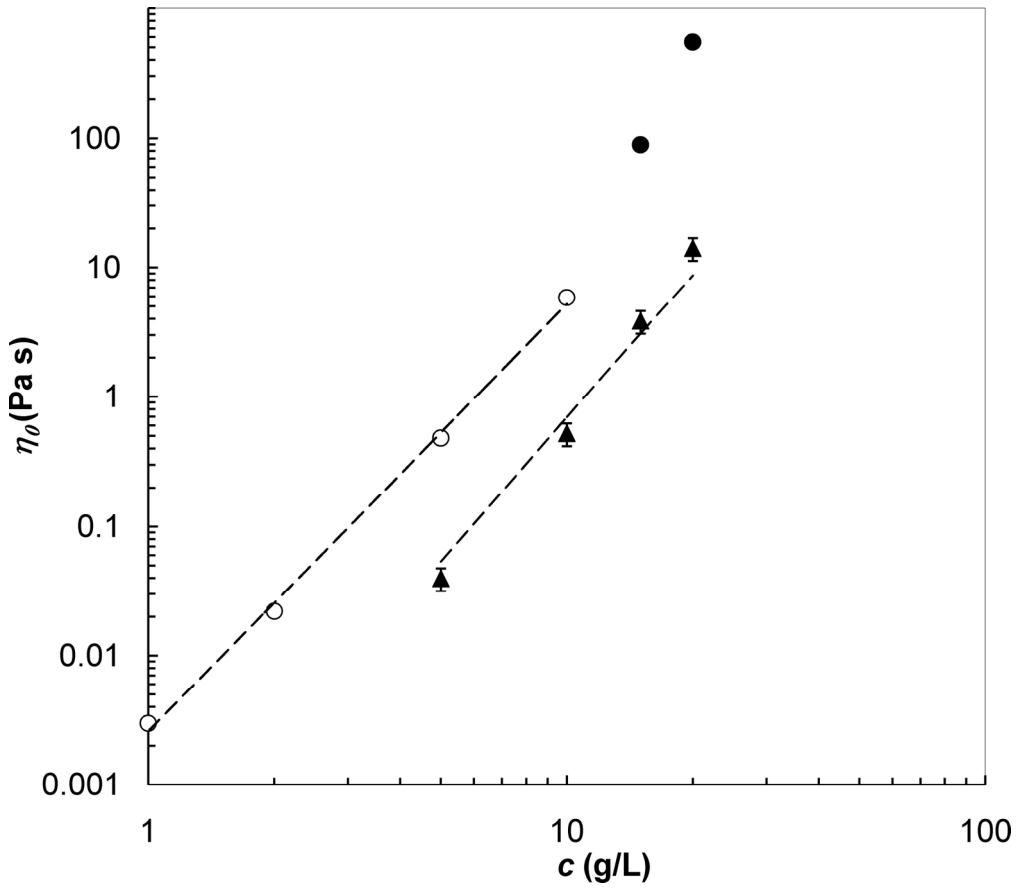

Figure 3a. Effect of concentration on Giesekus model parameter η_0 for guar gum and κ/ι-hybrid carrageenan gum. Dashed loci shows the power law trend line, Equation (24), fitted to the data for solutions in the semi-dilute regime, parameters given in Table 1. Symbols: circles – guar gum solutions, triangles - κ/ι-hybrid carrageenan gum solutions.
165x144mm (300 x 300 DPI)

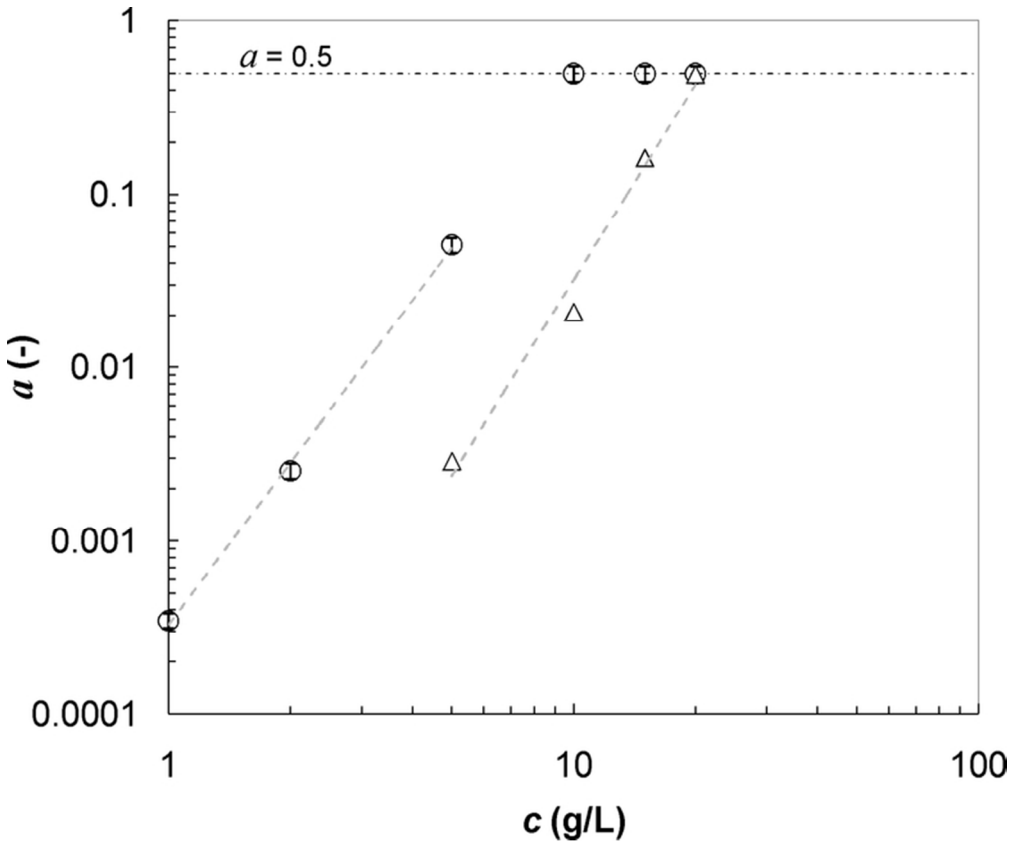

Figure 3b. Effect of concentration on Giesekus model parameter a for guar gum and κ/ι-hybrid carrageenan gum. Dashed loci shows the power law trend line, Equation (24), fitted to the data for solutions in the semi-dilute regime, parameters given in Table 1. Symbols: circles – guar gum solutions, triangles - κ/ι-hybrid carrageenan gum solutions.
65x54mm (300 x 300 DPI)

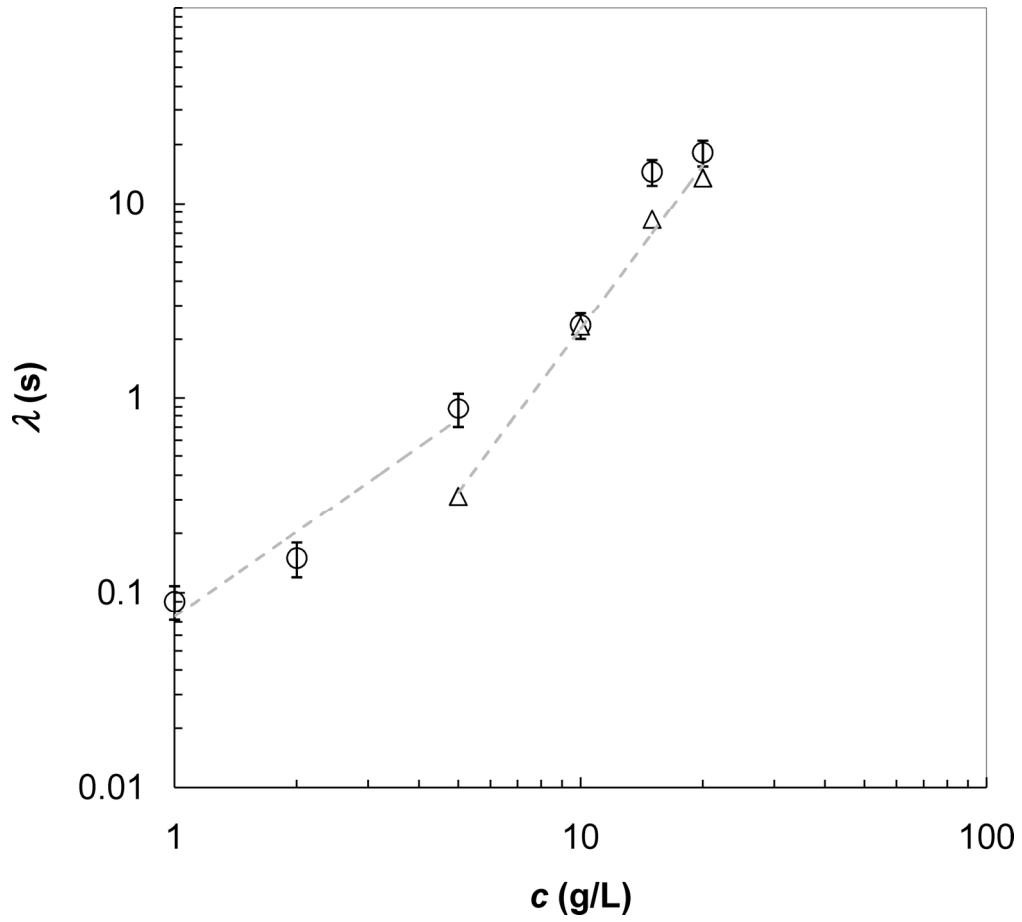

Figure 3c. Effect of concentration on Giesekus model parameter λ for guar gum and κ/ι-hybrid carrageenan gum. Dashed loci shows the power law trend line, Equation (24), fitted to the data for solutions in the semi-dilute regime, parameters given in Table 1. Symbols: circles – guar gum solutions, triangles - κ/ι-hybrid carrageenan gum solutions.
169x153mm (300 x 300 DPI)

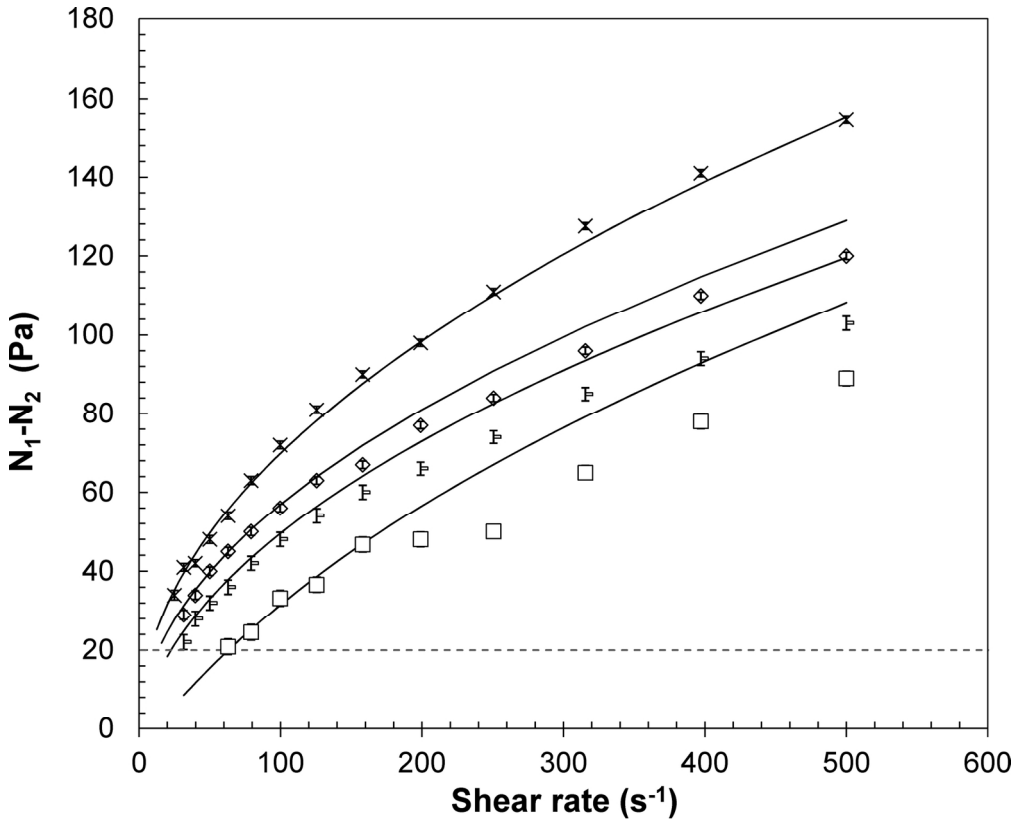

Figure 4a. Normal stress differences (N_1-N_2) measured for aqueous κ/ι-hybrid carrageenan gum solutions prepared at different polymer concentration. Lines show the difference between Equations (7) and (8) fitted to the data for studied solutions. Concentration: 2 g/L (open black triangles); 5 g/L (open grey squares); 10 g/L (open black diamonds); 15 g/L (dashes) and 20 g/L (crosses). The dashed horizontal line corresponds to the noise floor of the normal force transducer.
158x128mm (300 x 300 DPI)

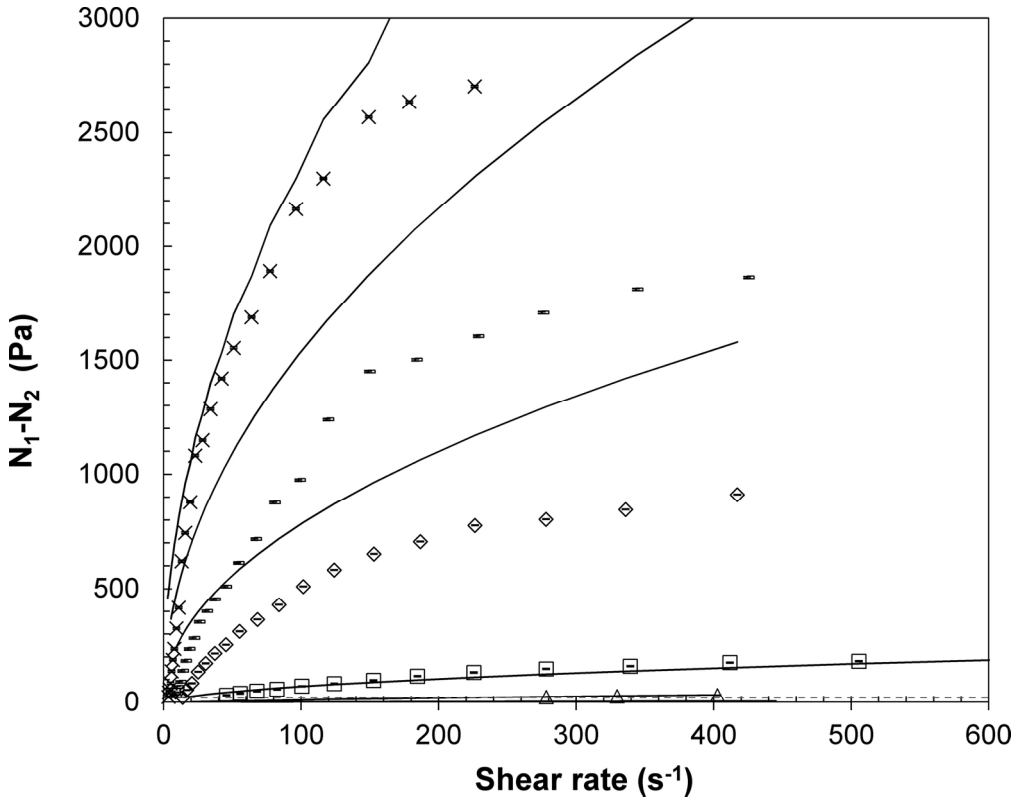

Figure 4b. Normal stress differences (N_1-N_2) measured for aqueous guar gum solutions prepared at different polymer concentration. Lines show the difference between Equations (7) and (8) fitted to the data for studied solutions. Concentration: 2 g/L (open black triangles); 5 g/L (open grey squares); 10 g/L (open black diamonds); 15 g/L (dashes) and 20 g/L (crosses). The dashed horizontal line corresponds to the noise floor of the normal force transducer.
160x126mm (300 x 300 DPI)

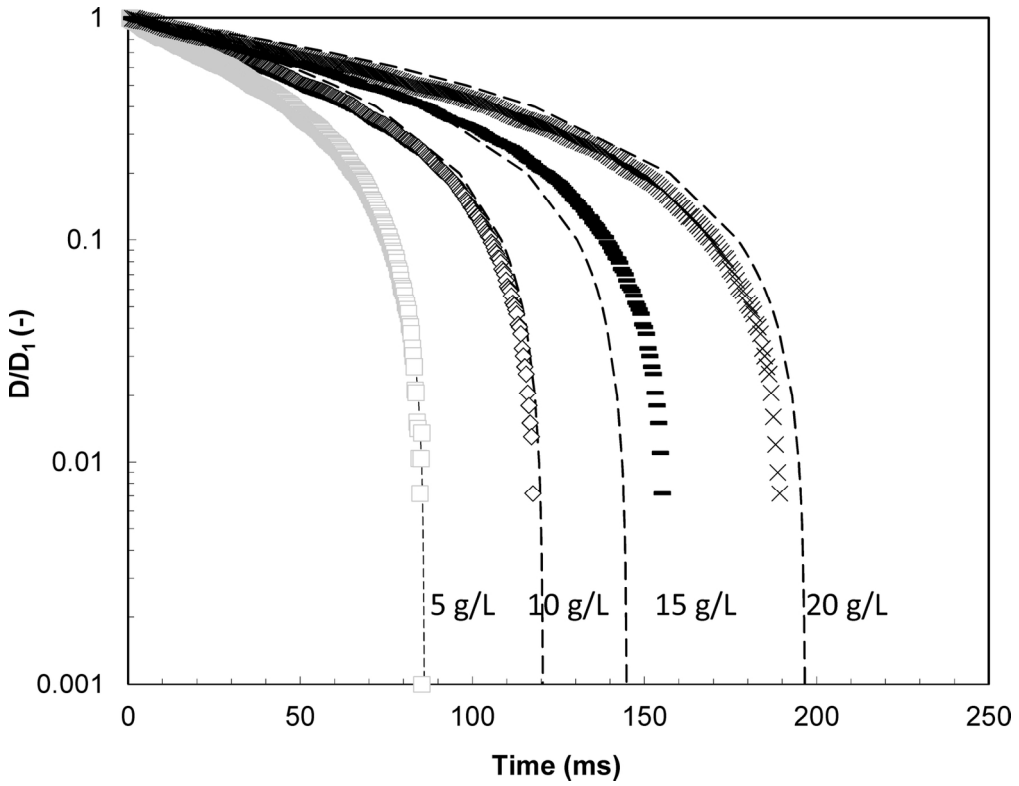

Figure 5a. Comparison of measured non-dimensional filament diameter with Giesekus model, Equation (19) for κ/ι-hybrid carrageenan gum solutions. Concentration: 1 g/L (open grey circles); 2 g/L (open black triangles); 5 g/L (open grey squares); 10 g/L (open black diamonds); 15 g/L (dashes) and 20 g/L (crosses). Dashed loci show predictions from Equation (19) using the parameters obtained from steady shear studies given in Table 1.
147x114mm (300 x 300 DPI)

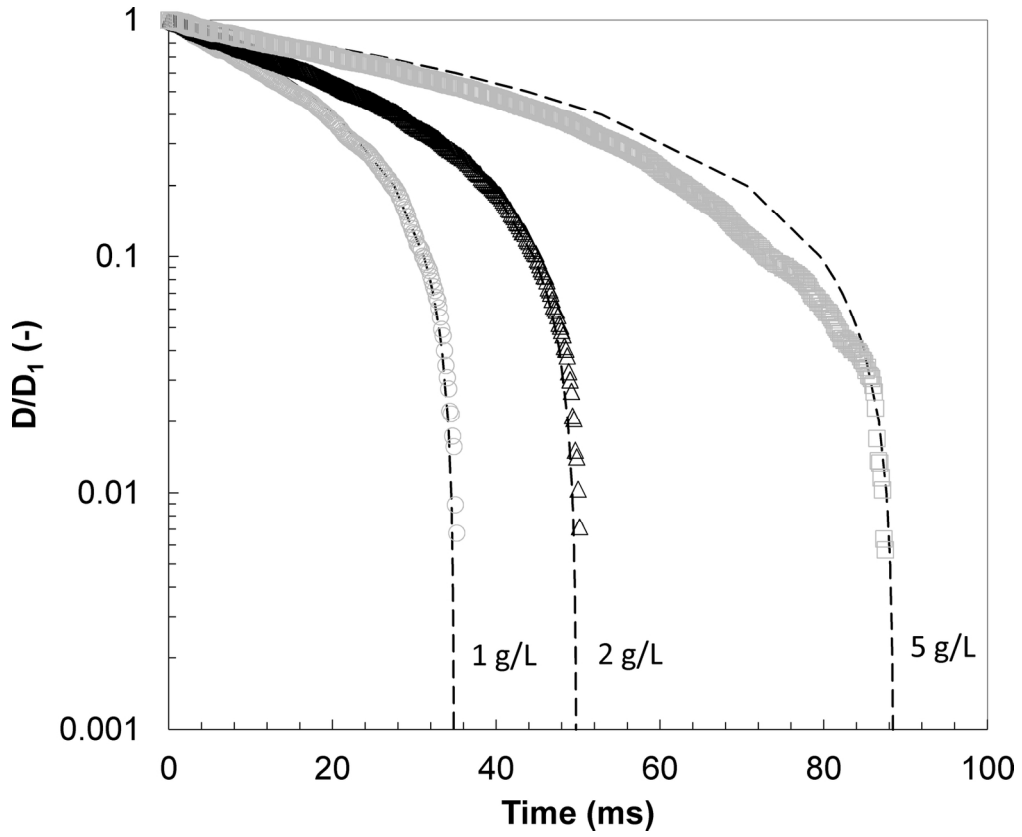

Figure 5b. Comparison of measured non-dimensional filament diameter with Giesekus model, Equation (19) for guar gum solutions, semi-dilute regime. Concentration: 1 g/L (open grey circles); 2 g/L (open black triangles); 5 g/L (open grey squares); 10 g/L (open black diamonds); 15 g/L (dashes) and 20 g/L (crosses). Dashed loci show predictions from Equation (19) using the parameters obtained from steady shear studies given in Table 1.
149x123mm (300 x 300 DPI)

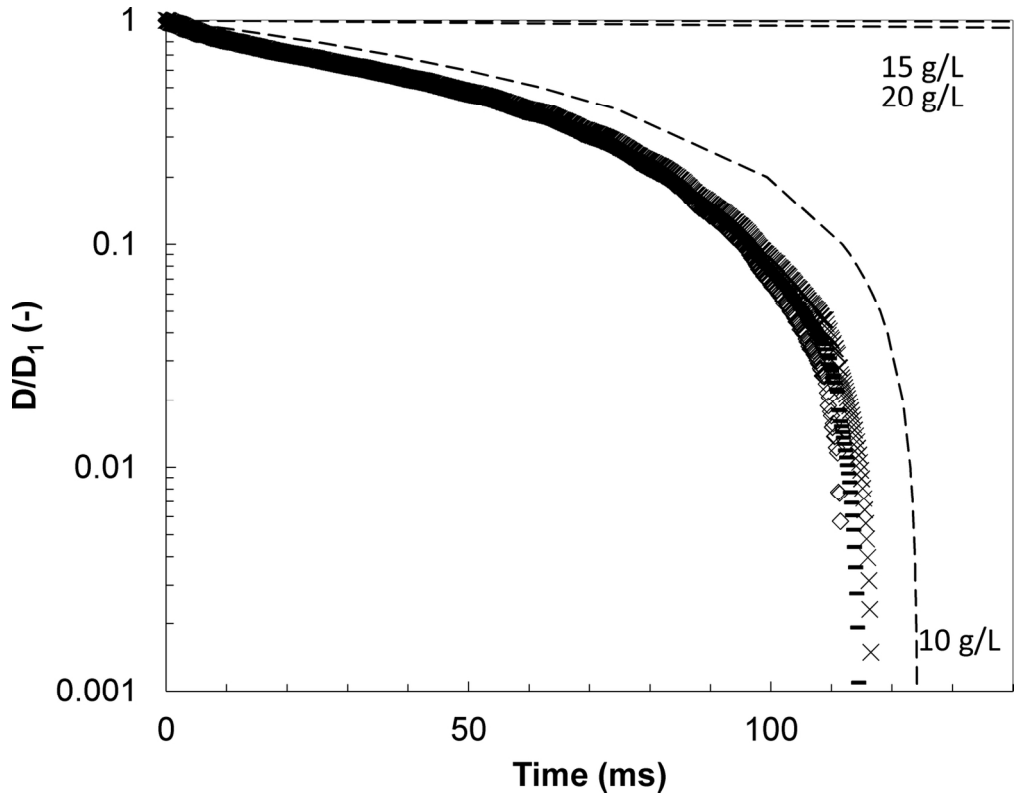

Comparison of measured non-dimensional filament diameter with Giesekus model, Equation (19) for guar gum solutions, entangled regime. Concentration: 1 g/L (open grey circles); 2 g/L (open black triangles); 5 g/L (open grey squares); 10 g/L (open black diamonds); 15 g/L (dashes) and 20 g/L (crosses). Dashed loci show predictions from Equation (19) using the parameters obtained from steady shear studies given in Table 1.
141x111mm (300 x 300 DPI)

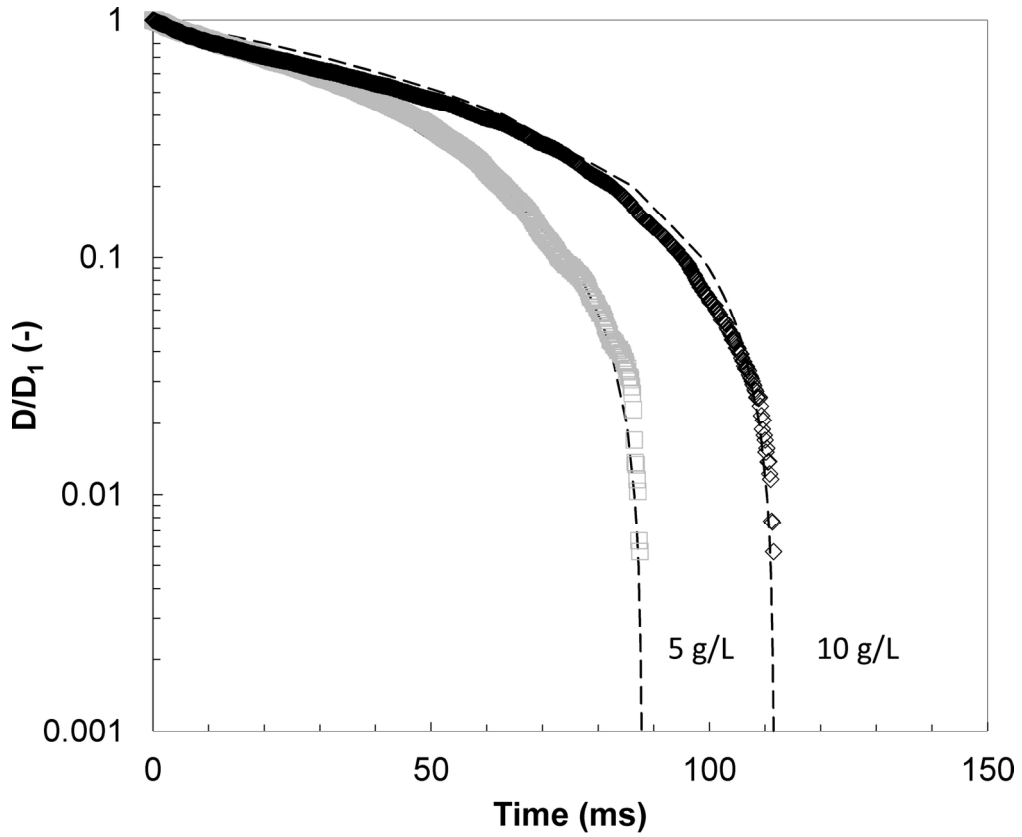

Figure 6. Fitting of guar gum solution filament stretching data in Figure 4(c) to Equation (19) when Giesekus model parameters a and λ are allowed to differ from those obtained from fitting shear flow data (Figure 2(a)). Dashed loci – model fit with parameters given in Table 3.
148x122mm (300 x 300 DPI)

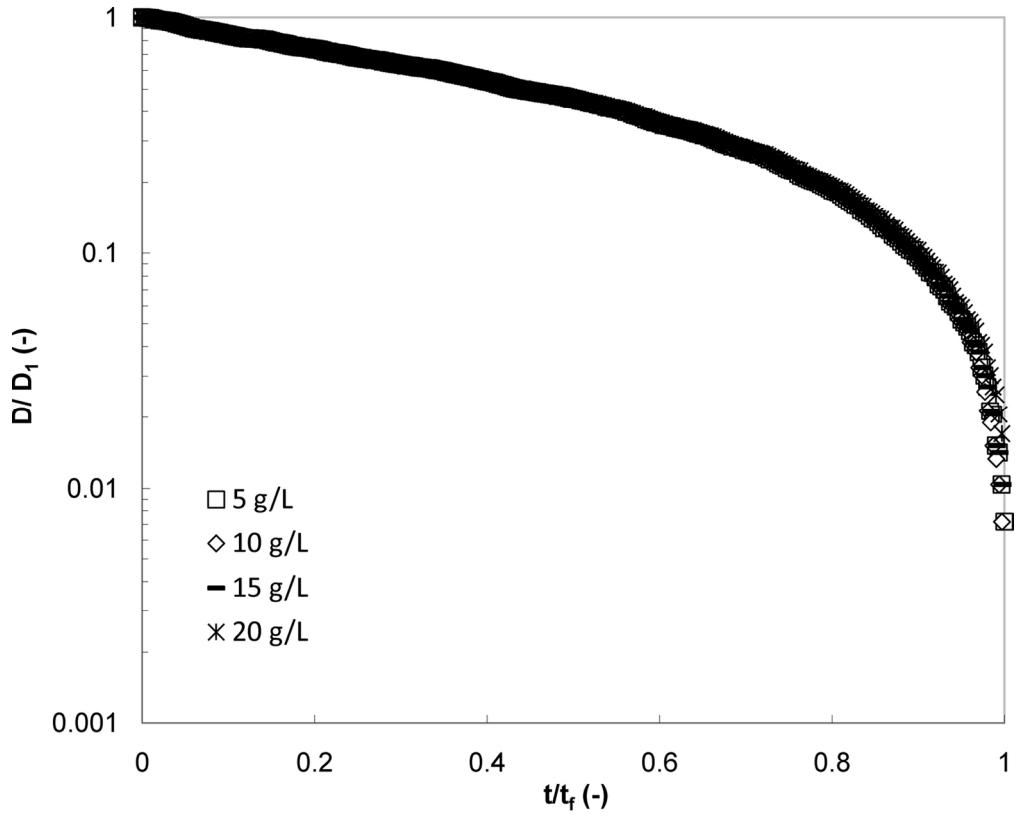

Figure 7a. Time-concentration superposition of the filament stretching data in Figure 5, where time is normalised by the experimental filament rupture time: κ/ι-hybrid carrageenan gum
68x54mm (600 x 600 DPI)

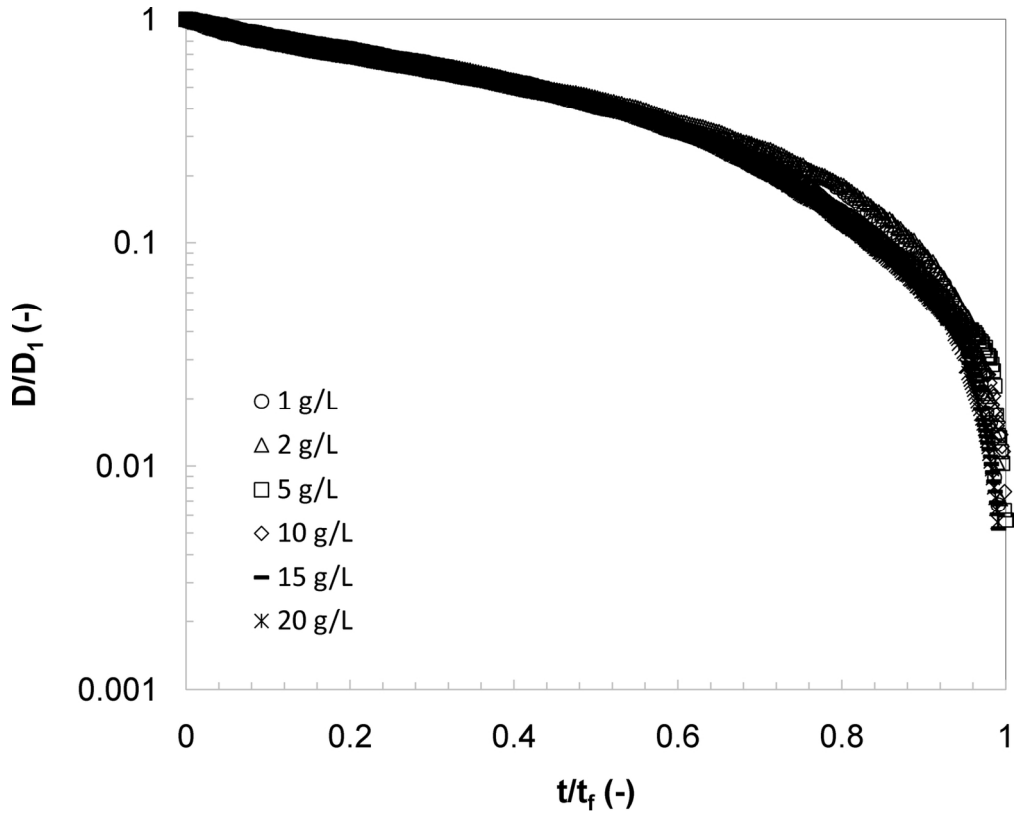

Figure 7b. Time-concentration superposition of the filament stretching data in Figure 5, where time is normalised by the experimental filament rupture time: guar gum (reproduced from Torres and co-workers [1]).
68x54mm (600 x 600 DPI)

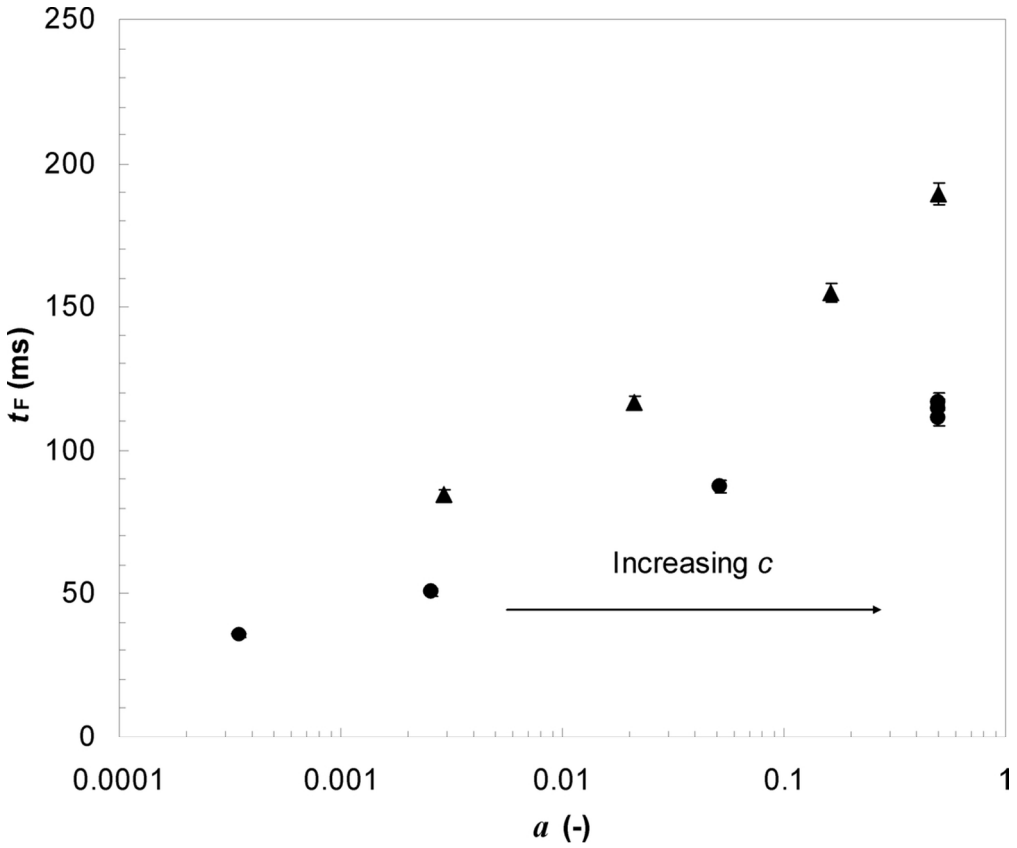

Figure 8. Relationship between filament rupture time, obtained from extensional testing, and mobility parameter obtained from shear flow data. Symbols: circles – guar gum, triangles - κ/ι-hybrid carrageenan gum solutions
104x87mm (300 x 300 DPI)

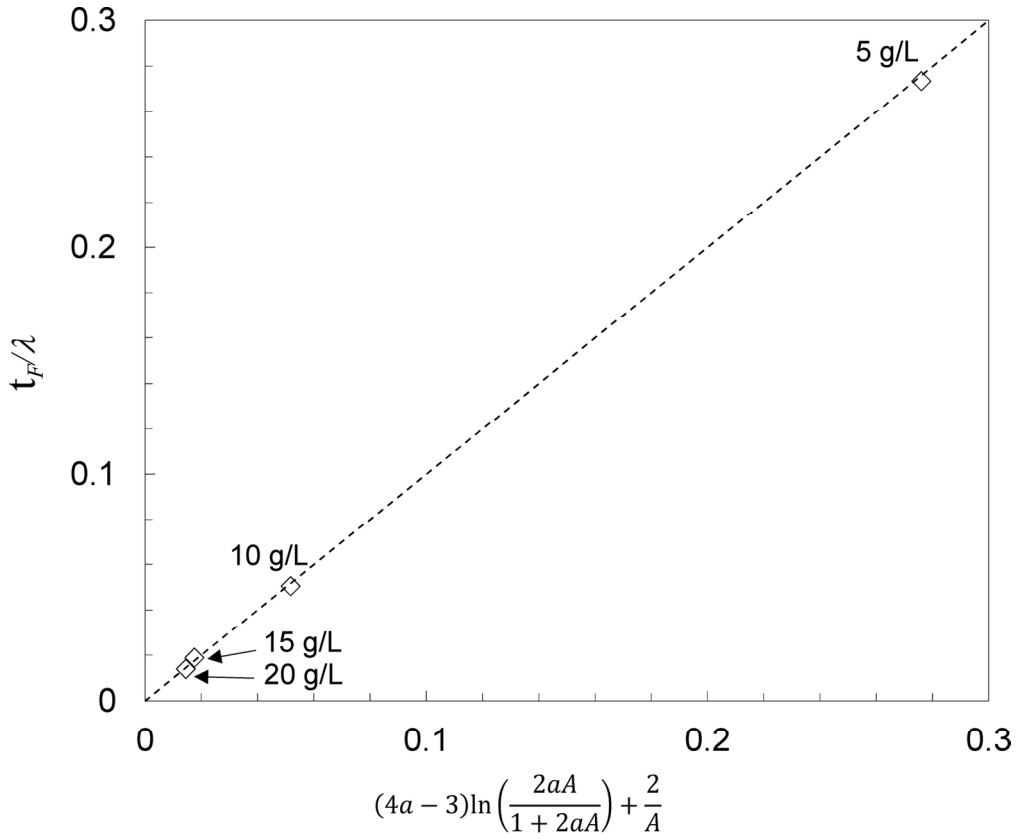

Figure 9a. Comparison of the left- and right-hand sides of Equation (25) for κ/ι-hybrid carrageenan gum solutions. Labels indicate gum concentration
146x121mm (300 x 300 DPI)

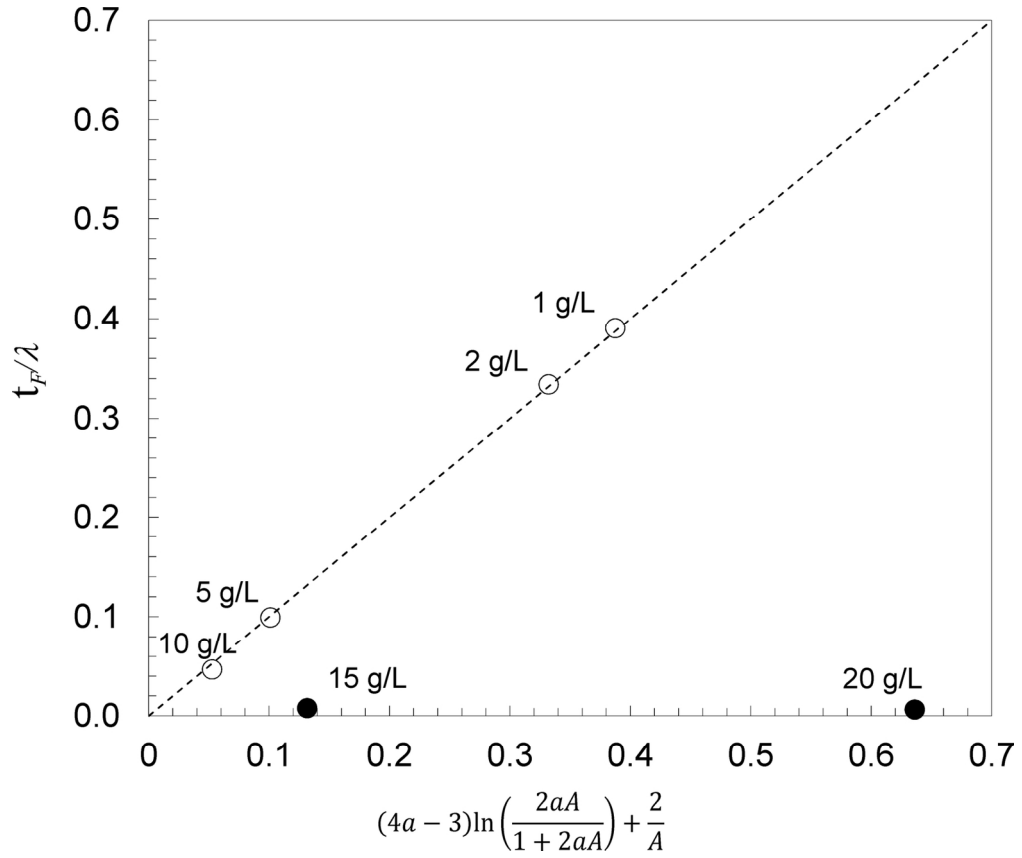

Figure 9b. Comparison of the left- and right-hand sides of Equation (25) for guar gum solutions. Open circles – guar gum in semi-dilute region; solid circles – guar gum in entangled regime. Labels indicate gum concentration
146x123mm (300 x 300 DPI)

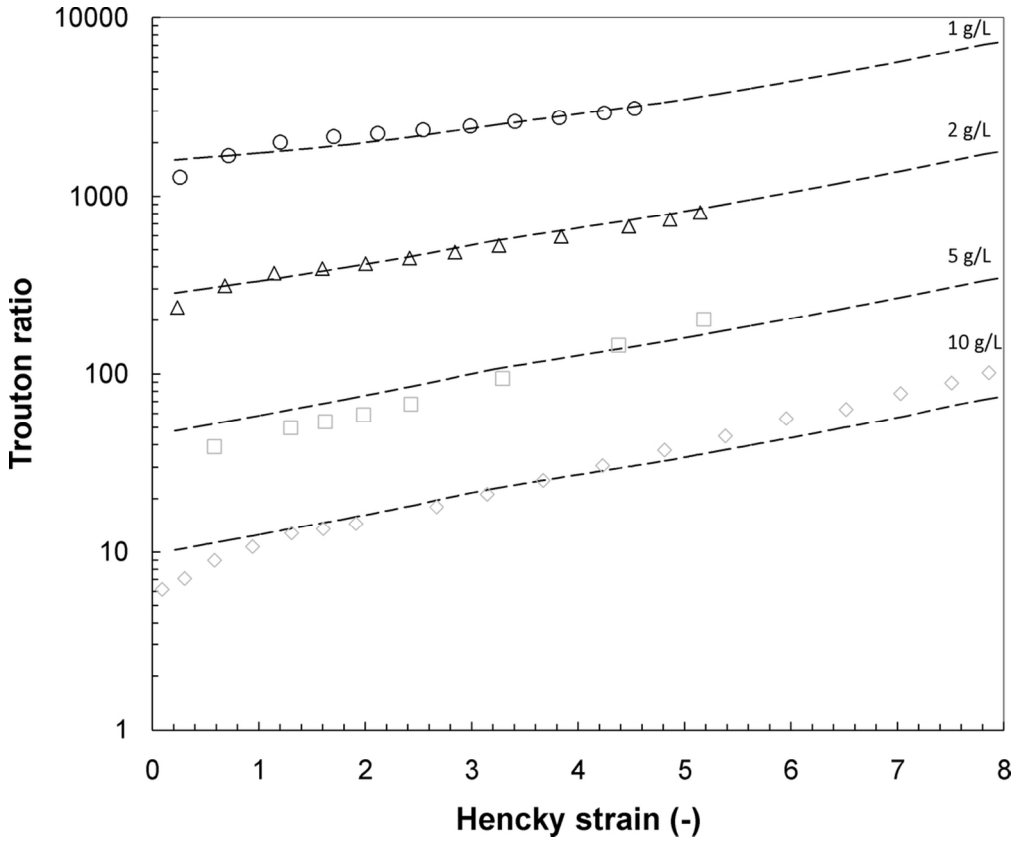

Figure 10. Effect of Hencky strain on Trouton ratio, for different guar gum concentrations. Symbols show experimental data reported by Torres and co-workers[1]. Solid loci represent predictions of the Trouton ratio via Equation (4) and Equation (22)
99x82mm (300 x 300 DPI)

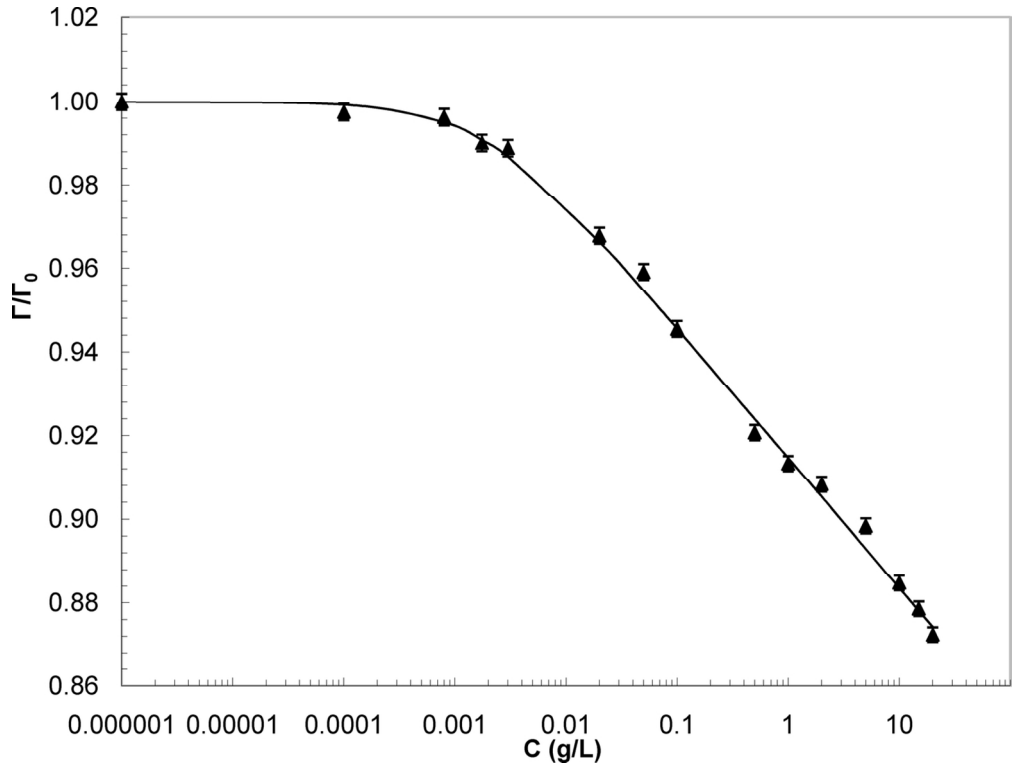

Figure A1. Effect of κ/ι-hybrid carrageenan gum concentration on surface tension relative to water. Solid trend line shows Equation (A.1) fitted to the κ/ι-hybrid carrageenan gum data with parameters s_1 = 0.0135 and s_2 = 0.0018 g/L.
61x46mm (600 x 600 DPI)

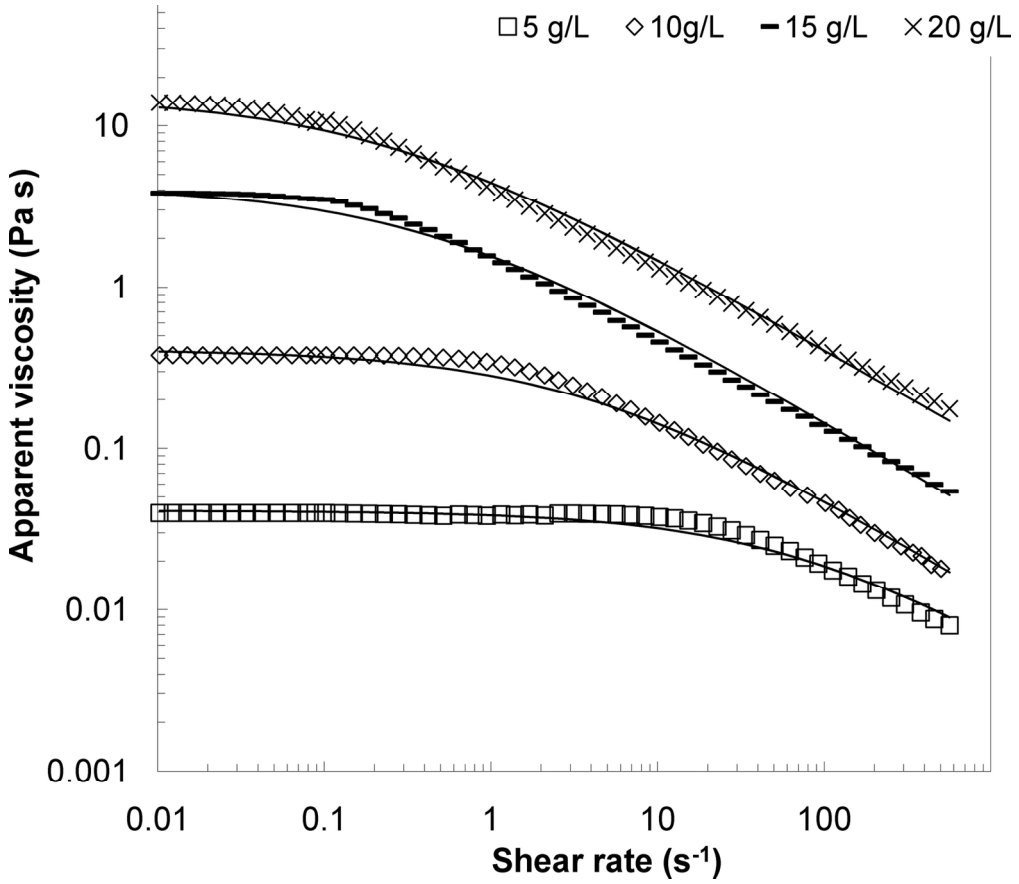

Figure A2. Flow curves of representative aqueous κ/ι-hybrid carrageenan gum solutions prepared at different concentrations. Symbols: 5 g/L (squares); 10 g/L (diamonds); 15 g/L (dashes) and 20 g/L (crosses). Dashed loci indicate model fit obtained using Cross model, Equation (A.2), parameters in Table A.1.
73x64mm (600 x 600 DPI)

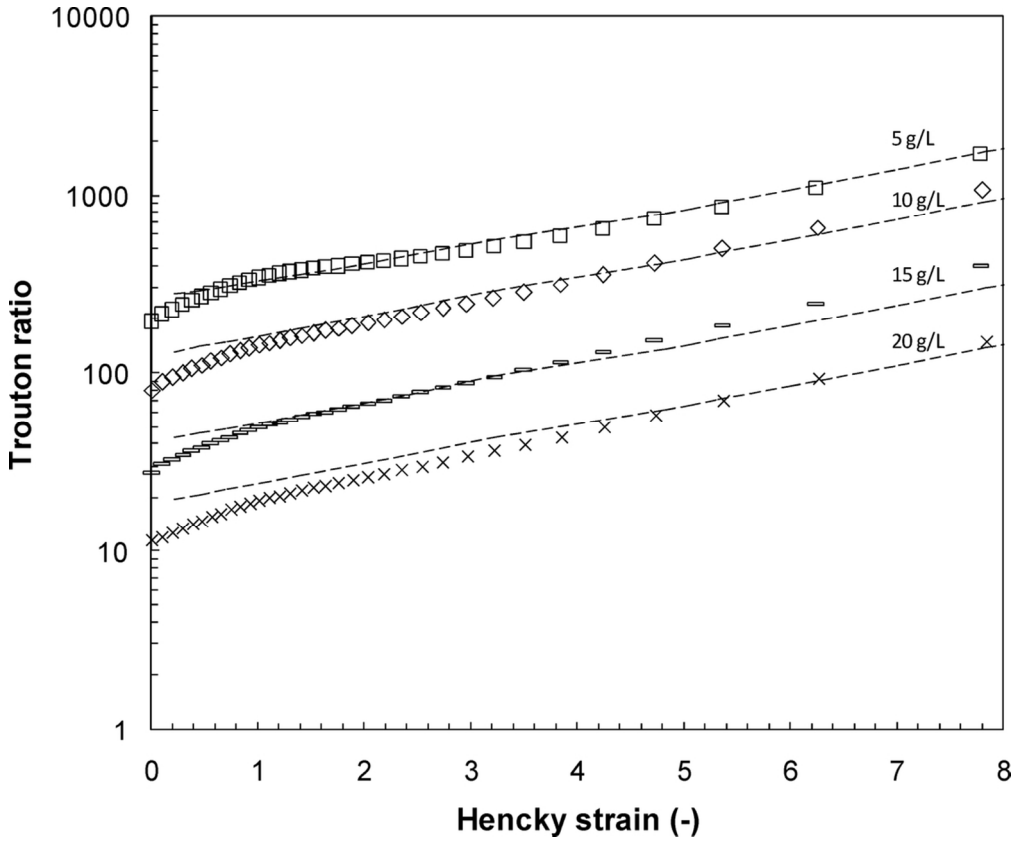

Figure A3. Effect of Hencky strain on Trouton ratio, for different κ/ι-hybrid carrageenan gum concentrations. Symbols: 5 g/L (squares); 10 g/L (diamonds); 15 g/L (dashes) and 20 g/L (crosses). Solid loci represent predictions of the Trouton ratio via Equation (4) and Equation (21)
99x82mm (300 x 300 DPI)